Ultrasonics Sonochemistry 95 (2023) 106399

Contents lists available at ScienceDirect

Ultrasonics Sonochemistry

journal homepage: www.elsevier.com/locate/ultson

Review

Research on synergistic erosion by cavitation and sediment: A review

Jie Sun [a], Xinfeng Ge [a,*], Ye Zhou [b], Demin Liu [c], Juan Liu [b], Gaiye Li [a], Yuan Zheng [a]

[a] Hohai University, Nanjing 210098, China
[b] Institute for Hydraulic Machinery, China Institute of Water Resources and Hydropower Research, Beijing 100038, China
[c] Dongfang Electric Machinery, Deyang 618000, China

ARTICLE INFO

Keywords:
Particle erosion
Cavitation damage
Synergistic effect
Dual mechanism
Numerical techniques

ABSTRACT

Sediment erosion frequently occurs in areas with high incidences of cavitation. The collaborative impact of abrasion and cavitation presents a host of challenges, threats, and damages to hydraulic engineering. However, little is known about the synergistic wear mechanism, and research conclusions remain inconsistent. In this work, relevant studies on synergistic erosion have been collected, classified, and analyzed. Presently, research on synergistic wear primarily operates at the macro and micro levels. The microscopic level enables the visualization and quantification of the process by which particles gain momentum from bubbles, the trajectory of particle acceleration, and the mechanism that triggers strong interactions between bubble-particle. At the macro level, erosion is understood as the summation of damage effects on the wall that is caused by the interaction between a plethora of bubbles of varying scales and numerous particles. The synergistic bubble-particle effect is reflected in the dual inhibiting or promoting mechanism. Furthermore, while numerical simulations could be realized by coupling cavitation, multiphase flow, and erosion models, their accuracy is not infallible. In the future, the dual role of particles, and particles driven by micro-jets or shock waves should be fully considered when establishing a combined erosion model. In addition, enhancing the influence of flow field and boundary parameters around bubbles and utilizing FSI would improve the predictive accuracy of erosion location and erosion rate. This work helps to elucidate the combined wear mechanism of hydraulic machinery components in sediment-laden flow environments and provides a theoretical basis for the design, manufacture, processing, and maintenance of hydraulic machinery.

1. Introduction

Statistics show that hydropower energy accounts for approximately 17% of the world's electricity demand [1], making up more than 72% of renewable energy sources [2]. In Latin America, approximately 65% of electricity is generated by hydropower plants [3]. This underscores the critical importance of hydropower as a sustainable and eco-friendly energy source for global electricity production. As a renewable energy resource with considerable developmental potential, excellent scalability, and mature technology, the further development and utilization of hydropower resources is a crucial aspect of future energy development worldwide. However, the excessive sedimentation in rivers such as those found in the Himalayas, Alps, and Andean regions is a significant challenge to the sustainable development of hydropower [4]. Sediment erosion during operation is a persistent problem in developed hydropower, while sediment deposition cannot be ignored for undeveloped hydropower. Thus, the issue of sediment erosion in hydraulic machinery remains an ongoing challenge for the foreseeable future. Additionally, the changing working conditions of hydro-turbines can cause cavitation erosion damage. The combined impact of erosion and cavitation presents a significant damage for hydraulic engineering [5,6].

In general, sediment erosion is characterized as the gradual removal of materials caused by abrasive wear [7]. The intensity of sediment erosion is dependent on three factors: (a) particle size, shape, hardness,

Abbreviations: HPS, hydroelectric power station; HVOF, high velocity oxyfuel spraying; FSI, fluid structure interaction; FVM, finite volume method; CFD, computational fluid dynamics; RNG, renormalization group; RANS, reynolds averaged navier-stokes; SCADA, supervisory control and data acquisition; MRPF, magnetorheological polishing fluid; GSC, green silicon carbide; STPs, silt-sized particles; LES, large eddy simulation; SST, shear stress transfer; VOF, volume of fluid; DNS, direct numerical simulation; ZGB, zwart gerber blemari; AHP, analytic hierarchy process; PSO, particle swarm optimization; SOM, self-organizing map; CIP, carbonyl iron particles; SDPs, sand-sized particles.

* Corresponding author.
E-mail address: gexinfeng@hhu.edu.cn (X. Ge).

https://doi.org/10.1016/j.ultsonch.2023.106399
Received 9 February 2023; Received in revised form 21 March 2023; Accepted 3 April 2023
Available online 5 April 2023

concentration, velocity, and collision angle [8]; (b) material hardness, chemical composition, microstructure, and strain hardening properties [9]; (c) fluid velocity, acceleration, flow medium, temperature, and turbulence [10]. Despite the various control measures employed by hydropower stations to remove particles, particles smaller than 10–60 μm are typically present in the flow in a suspended state. These tiny particles readily acquire energy from the turbulent structure of the boundary layer and repeatedly strike the walls, causing damage to the flow components [11]. Sediment erosion not only leads to a reduction in hydraulic machinery efficiency, resulting in noise and vibration and unexpected unit shutdowns, but also shortens the maintenance cycle and increases maintenance costs [12-15]. Moreover, material damage caused by sediment wear can alter the shape of components, causing or exacerbating cavitation damage [10,16].

It is widely recognized that pure water does not exhibit cavitation [17]. However, natural water contains numerous small nuclei composed of gas atoms. Cavitation refers to the formation, growth, and collapse of vapor or bubbles in a liquid or at the liquid–solid interface when the local pressure is reduced to the saturated vapor pressure of the liquid. In the low-pressure region, cavitating flow carries a significant number of bubbles to form a two-phase flow. When the cavitating flow passes through the high-pressure region, the bubbles collapse [18]. At low ultrasonic frequencies (e.g., 20 kHz), the oscillation and collapse of cavitation bubbles can generate intense shear forces, microjets, microflows, and shock waves [19]. Cavitation erosion is typically regarded as a fatigue failure caused by surface material damage due to microjets and shock waves [20]. The mechanism and impact of cavitation damage have been studied for a century [11,21,22]. Cavitation erosion is related to metal hardness[23], phase transition properties [24], work hardening [25], ambient temperature [26], corrosion resistance [27], coating [28,29], and other factors. The magnitude and direction of momentum carried by the jet flow are dependent on the dynamic characteristics of the cavity [30], the relative position of the wall, and the material properties of the wall [31,32]. It is commonly believed that sediment-laden flow has a higher critical cavitation coefficient than clear water, making it more prone to cavitation [33,34].

Sediment erosion often occurs in highly cavitated regions in the field [36], and the combination of sediment wear and cavitation erosion can lead to more severe damage [37], but the underlying mechanism is not well understood. Researchers have been investigating the relationship between cavitation and sediment wear since 1948 when Weyl and Marboe suggested that particles could promote cavitation [38]. In 1986, Jin et al. found that in addition to sponge-like wear caused by cavitation, particles could also cause craters, cracks, and cutting on the surface of turbines [39]. Wood et al. in 1990 [40] and 1991[41] confirmed the existence of synergistic wear by collecting large amounts of data, showing that the presence of particles amplifies cavitation damage. Madadnia and Owen conducted a test in 1993 that confirmed the promoting effect of bubble collapse on sediment erosion in fluidic valves controlling sand-laden water [42]. Subsequent experiments have commonly demonstrated that an increase in the quantity of cavitation nuclei present in the sediment-laden water flow leads to a mutually reinforcing relationship between cavitation and sediment erosion [43]. The combined wear strength of the two is generally greater than the damage caused by either one alone on the material [44,45], and in a specific environment, the combined wear effect can even reach 16 times that of pure cavitation wear [46] (see Fig. 1).

In the past two decades, the application of high-speed photography has facilitated the observation of the mechanisms by which particles are propelled during the expansion or collapse of a bubble, thereby enabling the exploration of the microscopic interplay between particles and cavitation [47]. As a result, previous assumptions regarding the mutual reinforcement of cavitation and sediment erosion have been overturned and dismissed. The synergistic effect between them is affected by bubbles, particles, and material properties [45,48-51]. The particles can have both promoting and inhibiting effects on cavitation. The combination of sediment abrasion and cavitation affect erosion rates by altering fluid viscosity [11,52], mixture kinetic energy [13], number of bubble nuclei [53], and bubble size [54], thereby complicating the prediction and evaluation of surface wear of materials. Despite numerous studies aimed at understanding the synergistic effect (as shown in Fig. 2), this question remains incompletely understood.

This paper presents a review of the synergistic erosion of particles and bubbles. Its objective is to comprehend the combined wear mechanism of hydraulic machinery components in a sediment-laden flow environment, and to provide a theoretical basis for the design, manufacturing, processing, maintenance of hydraulic machinery, as well as the safe, stable and optimal operation of power plants. The paper is structured as follows: Section 2 describes a field study that characterizes the combined wear phenomenon of three typical hydraulic machinery types, namely the impulse turbine, reaction turbine, and pump. Sections 3 and 4 investigate the synergistic mechanism and associated influencing factors from both micro and macro perspectives. Section 5 provides a summary of several representative combined erosion models developed in recent years. Section 6 describes advanced numerical simulation techniques of synergistic erosion, the selection of appropriate computation models, and addressing several challenging problems in numerical simulation research.

2. Field study

Synergistic erosion phenomena have been observed in various

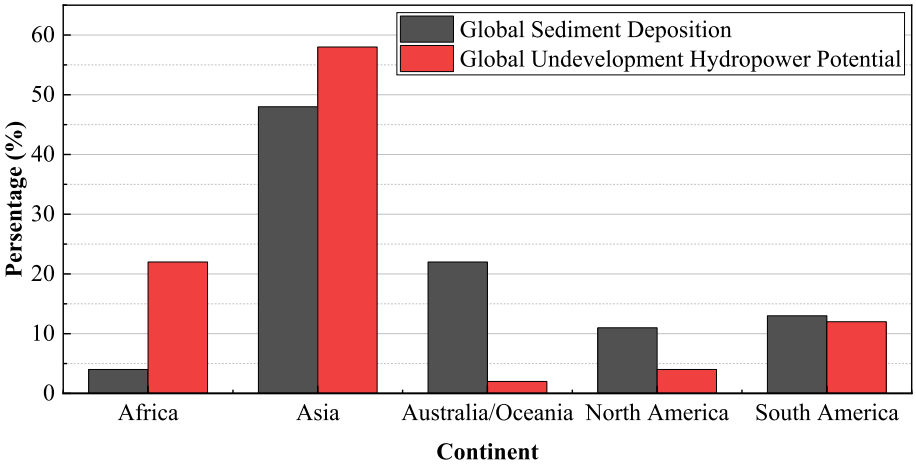

Fig. 1. Global percentage of undeveloped hydropower and annual sediment load deposition (Figures are recreated from ref. [35]).

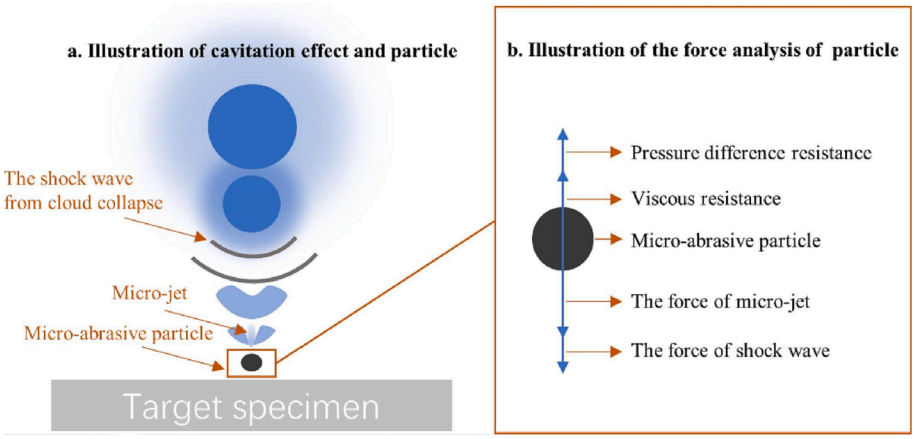

Fig. 2. Illustration of cavitation effect and particle [55].

hydraulic machineries, such as the injector and runner of Pelton turbines [56,57], the runner blade [58], and anti-wear rings [59] of Francis turbines, as well as the front shroud and pump casing of slurry pumps [60]. The wear is particularly pronounced in areas where the flow-passing parts are cast with defects [61,62]. Synergistic erosion not only results in material loss, but also intensifies vibration in the vicinity of rotating parts [35], leading to increased failure and fatigue damage of the runner, higher maintenance costs, and greater economic loss [63]. While wear types are typically identified based on cavitation and sediment erosion characteristics on the material surface, distinguishing between them can sometimes prove challenging [64]. The following examples illustrate some typical cases of synergistic wear.

2.1. Impulse turbine

The Pelton unit is susceptible to sediment abrasion and cavitation erosion in sediment-rich rivers due to its high head [65,66]. To assess the wear of the Pelton turbine nozzle and needle under 365 m of head after 2712 h, the Chenani power plant employed 3D scanning technology [67]. The survey revealed that 67.37% of the particles in the river were 0.075 mm in size, and during the monsoon season, the maximum concentration of particles could reach 2 kg/m^3. Fig. 3 illustrates the needle erosion region, which can be divided into three zones: shallow corrugated erosion in zone I, pits and cracks in zone II, and serrated ripples in zone III. Zone III exacerbates the material loss and plastic deformation of the nozzle head, eventually leading to nozzle head fracture. In cases of combined erosion, the loss of needle volume can be as much as 3.71%. For the Kulekhani power station located in Nipol, cavitation contributes to erosion at a rate of about 0.5045 mm/year, while particles contribute at a rate of about 0.0046 mm/year [68]. Fig. 4 demonstrates that combined erosion damage to the material surface is extremely severe.

2.2. Reaction turbine

The category of reaction turbines comprises the Francis, tubular, and Kaplan turbines. Among these, the Francis turbine with an operational head ranging from 20 to 700 m, is particularly susceptible to synergistic wear, as observed in the Three Gorges and other power plants [69]. Notably, severe wear was found on the Francis turbine runner at the

Fig. 4. Erosion due to sand particles and cavitation (left Puwakhola HPS) and erosion due to cavitation (right Kulekhani HPS) in the bucket [68].

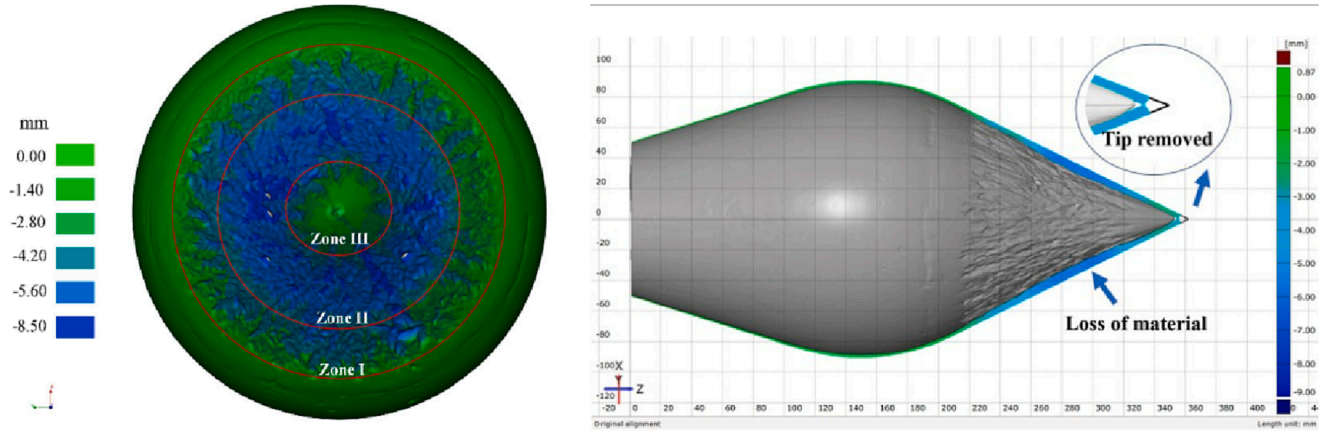

Fig. 3. Wear zones of the Chenani Hydro-Power Plant spray needle [67].

Amaime power plant after only six months of operation, as depicted in Fig. 5 [70]. This type of wear is often attributed to particle erosion and cavitation, given that sediment wear typically corresponds with cavitation locations [71,72]. The blade of the Muzhati III powerhouse in Aksubai, Xinjiang, as illustrated in Fig. 6, exhibited surface imperfections in the form of pits, fish-scale pits, and pinhole pits, with the blade's outer edge being broken [73]. During operation, high-speed small particles not only pass through the 200 gaps between the anti-wear plate and the guide vane but also contribute to loss caused by the horseshoe vortex [70]. At the Gongzui hydropower station, the stationary guide vane and stay ring display distinct cavitation failure pits and wear, which not only cause substrate damage but also lead to a severe decline in the support force of the guide vane [74].

2.3. Pump

Centrifugal pumps are commonly employed for the transportation of solid–liquid slurry [75], and in recent years, there has been an increased focus on the cavitation characteristics of pumps operating under sediment-laden conditions [76,77]. The interaction between the abrasive hydraulic flow and the surface is intensified by alternating and pulsating loads, leading to a 10% increase in pump wear and a 9% reduction in pump capacity [78]. Among the components, the impeller, liners, and pump casing are the most prone to wear, with the pump casing being particularly susceptible [79]. For instance, the axial flow pump in Uzbekistan suffered severe wear after 2680 h of operation, resulting in a thickness of only 0.3–0.5 mm at the inlet edge of the blade and a groove depth of up to 1.5 mm at the outlet edge [80]. Similarly, the pumps in Turakurgan-1 and Turakurgan-2 displayed serrated blade inlet edges and significant blade damage [81]. Moreover, a slurry pump in a Shanghai power plant exhibited severe wear on the front shroud after 12 months of operation (as shown in Fig. 7 (a)). Even after repair, the pump casing still experienced a wear depth of up to 10 mm after 36 months of operation (as shown in Fig. 7 (b)).

It is noteworthy that, on one hand, relying on field tests for wear assessment can be a time-consuming process, and the empirical formula based on field data may not always be widely applicable. On the other hand, identifying the specific factors that contribute to combined erosion through field tests can be a challenging task. Wear caused by particle abrasion and cavitation erosion is a common phenomenon in friction systems that involve bubbles and particles [82]. Therefore, understanding the mechanisms of erosion and identifying the factors that influence the erosion rate could help to enhance the durability of the eroded components, particularly from a design perspective [83]. Consequently, sections 3 and 4 of the present study aim to investigate the synergistic mechanism and relevant influencing factors at both microscopic and macroscopic levels.

3. Bubble-particle interaction at the microscopic scale

Nowadays, there is limited cognition regarding the damage caused by the collapse of bubble on fixed wall surfaces, and the interaction between cavitation and suspended particles is not yet fully recognized [84]. However, with advancements in science and technology, along with improvements in measuring instruments and accuracy, such as in ultrasonic cavitation measurement [85-89], it has become possible to comprehend the formation, aggregation, and interaction of particles and bubbles [90,91]. For instance, Mitra et al. observed two stages of bubble-particle attachment, which included the accumulation of hydrophobic particles formed by fine-sized cavitation bubbles through capillary bridging, and the collection of particle clusters by larger-sized carrier bubbles [92]. The microscopic mechanism can be divided into two categories based on the research objects [93]: (a) particle behavior, which includes motion direction [94,95], self-rotation [96], and acceleration motion [97], and (b) bubble behavior, which includes nucleation [98], non-spherical collapse [99], and bubble jet flow [100].

The subsequent discourse delves into the microscopic-level

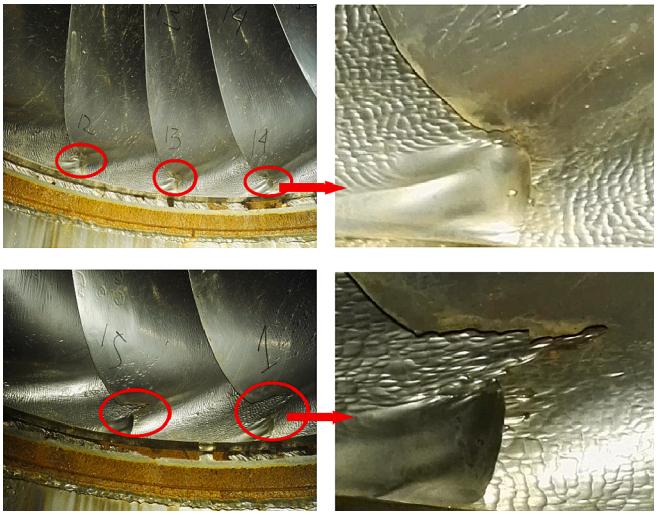

Fig. 6. Abrasion photo of runner blade of Muzhati III power station in Aksubai, Xinjiang [73].

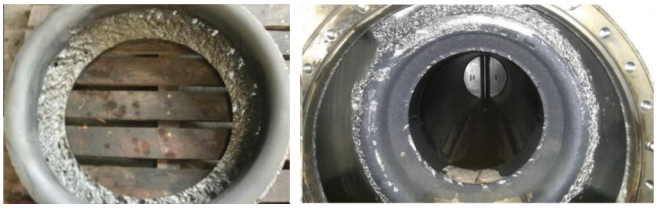

(a) Front shroud (b) Pump casing

Fig. 7. Wear of the front shroud and pump casing of a pump station in Shanghai [81].

Fig. 5. Wear on the Francis turbine at the Amaime hydropower plant after six months of operation [70].

interaction between bubbles and particles, encompassing the development of bubbles on particles, particle motion around bubbles, particle acceleration, cavitation-particle interaction, particle decomposition and destruction, and the deformation of both bubbles and particles during their interaction.

3.1. Development of bubble on a particle

Chang [101] conducted an examination of the cavitation process on a single particle surface (diameter: 0.69 mm) using a cavitation pressure tester, microscopic observation device, and digital video recorder equipment. The results demonstrated that with the decrease in water pressure, the small gas nuclei located within the particle cracks gradually expanded, attached, and even detached from the particle surface. In Arora's experimental investigation [102], it was determined that during the expansion process, the bubble would displace the surrounding particles and cause translational motion, and as the tensile stress decreases, the particles and bubble would ultimately separate.

Borkent et al. employed high-speed photography capturing 1 million frames per second to document the evolution of cavitation on particles, as depicted in Fig. 8 [103]. This progression can be categorized into three distinct stages: (a) the prompt expansion of the bubble on the surface of the particle (0–4.9 μs); (b) formation of a neck and subsequent separation (4.9–10.8 μs); (c) the collapse of the bubble followed by secondary expansion and the emergence of newly-attached cavitation on the particle surface.

The underlying mechanism behind the formation and growth of bubbles on particle surfaces is commonly attributed to the presence of gas stored in surface cracks on the particles, owing to capillary action [12,103]. When subjected to external stimulation, these cracks serve as cavitation nucleation sites, leading to the formation of bubbles. As the bubbles grow, they eventually detach from the particles due to tensile stresses. Notably, the cavitation activity exhibited by different particles varies [104], and is closely tied to the surface structural properties of the particles [105], such as roughness and hydrophobicity [102]. Interestingly, particle curvature does not appear to play a significant role in cavitation activity. In particular, hydrophobic particles possessing a corrugated surface topography exhibit a marked increase in cavitation activity, while hydrophilic and smooth particles are less effective in promoting cavitation [106,107]. Bubbles are able to rapidly form on hydrophobic surfaces with high contact angles, as higher contact angles reduce the energy barrier required to form cavities [108]. However, as the contact angle increases, the duration of bubble-particle adhesion decreases [109]. Moreover, the impact of environmental pressure on the bubble development process is substantial, as excessively high pressures serve to inhibit bubble growth [106].

Although particles move away from the nucleus in a specific direction as the bubble develops, the direction of their movement when separated from the bubble is determined by the cavitation nuclei distributed randomly over the particles, independent of the external

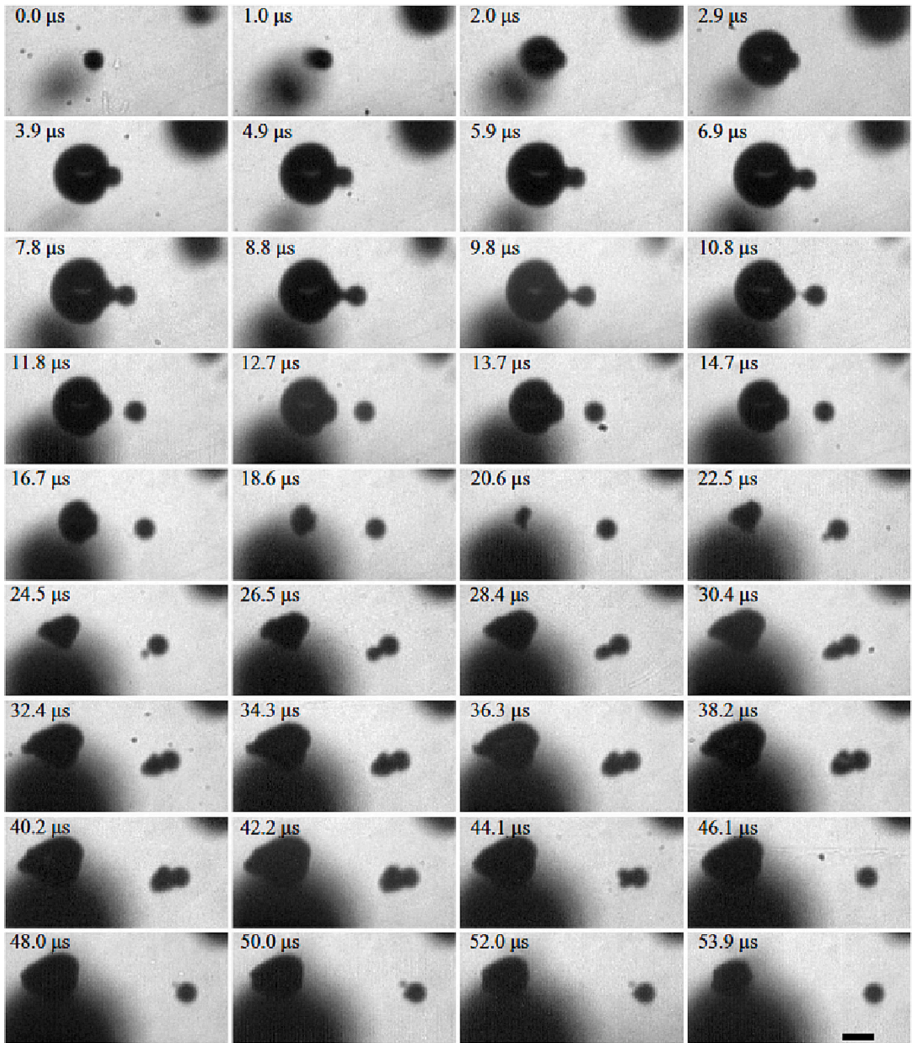

Fig. 8. Three stages of bubble development on particles [103].

environment. In addition to the typical growth and separation process of a single bubble on a particle, there are also instances where multiple bubbles grow simultaneously on the particle. In experiments, this phenomenon is observed with a probability of around 20% [103]. Fig. 9 illustrates that during the development of multiple bubble nucleation sites, bubbles will merge, leading to an expansion of the gas–liquid cross-section.

3.2. The motion of particles around the bubble

The preceding section outlines the formation and progression of bubbles on particles when nuclei are present within the cracks on the particle surface. However, in reality, when particles enter the cavitation region, the fluid surrounding the particles is prone to reaching the cavitation condition and generating bubbles. In such cases, the gas nuclei have an initial distance from the particles, and the motion process that ensues after the interaction between the bubble and particle is distinct from that in Section 3.1.

In the study conducted by Soh and Willis [31], the impact of particle position on particle motion in the vicinity of bubbles was investigated. Fig. 10 illustrates three types of particle positions near bubbles, including free-falling particles (A), suspended particles (B, C, D, E, F, G), and particles in contact with the wall (p6, p7). The results of the study indicate that during the process of bubble collapse, suspended particles and free-falling particles do not experience any significant motion, whereas particles in contact with the wall surface move vertically upward. Based on these observations, the researchers conclude that the material damage caused by particle motion is not due to the transient flow caused by bubble collapse, but rather due to the high contact force resulting from wall vibration after the bubble impacts the wall.

The assertion that bubbles are unable to exert a propulsive force on nearby particles such as free-falling or suspended particles was challenged by Li et al. They noted that the experimental findings of Soh and Willis may be attributed to the distance between the bubble and particle being too great to stimulate a substantial interaction governed by inertial forces [17]. Poulain's research corroborated this hypothesis, as he observed that the motion of particles was highly dependent on their initial separation distance from the bubble [84]. Even small differences in the starting positions of particles, by just 0.7 mm, resulted in over twice the variation in their subsequent displacement. Teran also noted that bubbles can induce a significant acceleration effect on neighboring particles during their growth and collapse, although this effect is negligible when the distance between them is sufficiently large [110].

To gain a better understanding of the motion behavior of particles that are suspended near bubbles, Poulain utilized a high-speed camera with a frame rate of 64,000 frames per second to document this evolutionary process (refer to Fig. 11) [84]. Through the use of spark-induced devices, he conducted a study on the interactions between bubbles and suspended particles in materials such as glass, aluminum, brass, and steel. He observed that the motion process between the bubble and the surrounding particles can be divided into three stages: (a) bubble generation, with the particles being pushed away during the expansion process; (b) bubble collapse, during which the surface of the bubble changes from spherical to non-spherical after reaching maximum volume; and (c) particle attraction as they approach during bubble collapse.

When examining the effect of bubbles on the movement of the surrounding particles, it is crucial to consider the initial relative position of the particles within the gaseous nucleus [112]. If the gas nucleus is located in the surface crack of the particle, there will be stronger repulsive forces acting on the particles during the bubble's evolution process, causing the particles to be pushed further away. Conversely, when the cavitation nucleus is situated in the water close to the particles, the particles experience repulsion during the bubble expansion stage and attraction during the bubble collapse stage. According to Gonzalez-Avila et al. [96], whether the particle is subject to attraction or repulsion is mainly dependent on the initial distance between the particle and the bubble. Through recording particle trajectories at varying initial distances and analyzing the relationship between particle displacement and initial distance, they were able to obtain a better understanding of this phenomenon.

3.3. Acceleration effect of bubble on particles

Based on the aforementioned research, it is evident that the bubble

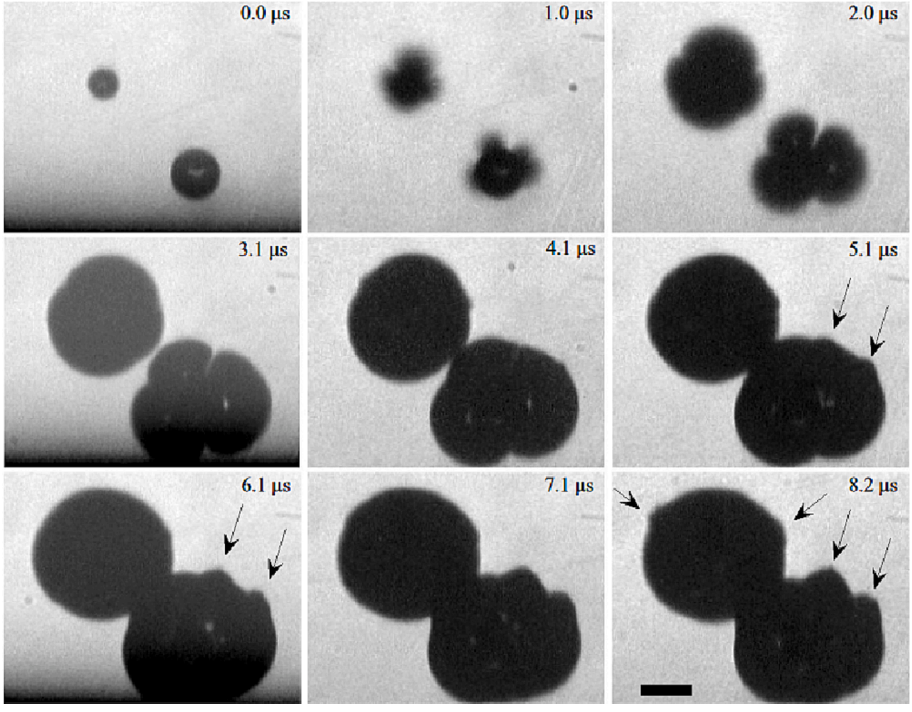

Fig. 9. Multiple starting points of cavitation on the particle [103].

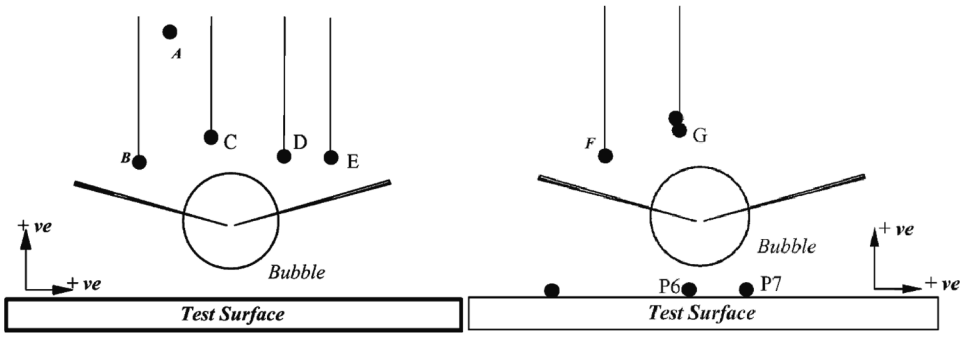

Fig. 10. Particle arrangement relative to the electrode in the test [31].

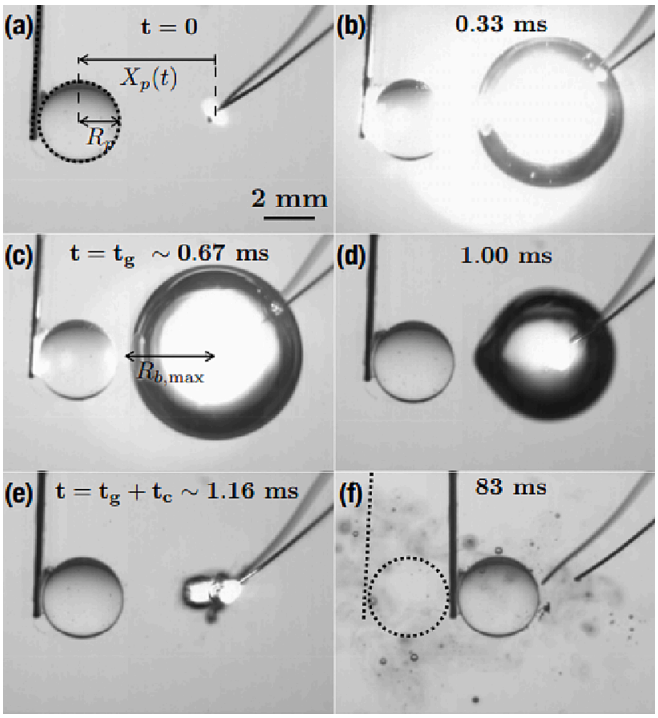

Fig. 11. Position of bubble and glass particle at different moments [84].

has a significant impact on both the attached particles and the neighboring particles during the evolution process, regardless of whether the cavitation nucleus is located in the particle crack or in the water. Specifically, the bubble generates attraction or repulsion to nearby particles during the stages of growth and collapse, resulting in particle acceleration and an increased erosion rate of material surface particles. Borkent et al. reported that during the expansion process, the bubble can accelerate particles to velocities of up to 40 m/s or even higher [103,113]. The most critical factors affecting particle velocity are the relative distance between particles and bubbles, the material type, and the particle size. Larger, denser alumina particles are more challenging to move than smaller, lighter particles [110]. Particles in close proximity to the bubble interface are more greatly affected by the velocity field generated by bubble growth and collapse, whereas those further from the bubble interface experience less impact [110].

In their experimental study, Wu et al. [114] investigated the relationship between laser-induced bubbles and settling particles, and explored the acceleration effect between the two. Building upon this, they established a force balance model for particle-bubble dynamics to predict the maximum velocity of particles. Results showed that when the distance between the particles and the bubbles is extremely small, the particles can experience acceleration exceeding 60 m/s, which is sufficient to cause plastic deformation of a stainless steel plate.

Xu et al. [115] investigated the impact of a single bubble on particle motion using a low-voltage electric spark discharge device to generate bubbles. They examined metal particles with diameters of 4.73 mm and 5.98 mm, respectively, and varied the liquid viscosity by adjusting the glycerol-water ratio. The study showed that particle velocity is influenced by fluid viscosity, particle size, and pipe diameter. Based on their findings, a model for predicting particle velocity is proposed.

Pavard et al. utilized the jet flow generated by bubble collapse to enhance particle motion, as demonstrated in Fig. 12 (a) and (b) where particles were placed on a transparent plate and a horizontal hole, respectively [116]. The momentum for particle motion was generated by the impinging jet flow, and the subsequent dynamics of the bubble influenced the particles in the water. Additionally, secondary acceleration was observed during this process.

Li et al. [17] conducted an experimental study where they observed the translational motion of particles induced by bubble expansion and the secondary acceleration process of particles by bubble collapse, as depicted in Fig. 13. Additionally, Gonzalez-Avila et al. [96] observed particle rotation during bubble expansion, in addition to particle acceleration.

Tan et al. [117] conducted a thorough investigation and analysis of the phenomenon of particle acceleration induced by cavitation-particle interactions in recent years. They hypothesized that the velocity of particles is highly dependent on both the mode of bubble generation and the physical properties of the particles themselves. Consequently, they developed a novel experimental technique to estimate particle velocity. Specifically, they positioned a ductile metal target sample at a short distance from the ultrasonic horn tip, enabling them to capture accelerating particles using the cavitation effect of a powerful ultrasonic system in a solid–liquid mixture. The average velocity of the particles was then estimated using the inverse solid particle erosion model's mass loss data. This innovative approach enhances our fundamental comprehension of the particle dynamics triggered by cavitation.

3.4. Interaction between bubble and multi-particles

The aforementioned studies primarily concentrate on the interaction between bubbles and individual particles. However, Chen et al. conducted an investigation on the interaction between bubbles and multiple spherical particles utilizing an ultrasound vibration cavitation instrument and a low-pressure underwater discharge device [118]. They observed that particle size has a direct correlation with erosion damage, with larger particles experiencing more damage. This result is reversed when the average particle size is less than 0.120 mm. Furthermore, an increase in particle concentration amplifies its impact on cavitation.

Additionally, they observed that when multiple spherical particles interacted with the bubble, it exhibited a non-spherical morphology, as shown in Fig. 14. This is due to the fact that the interaction between the bubble and small particles slows down the surrounding flow velocity, resulting in a prolonged cavitation time and reduced cavitation intensity

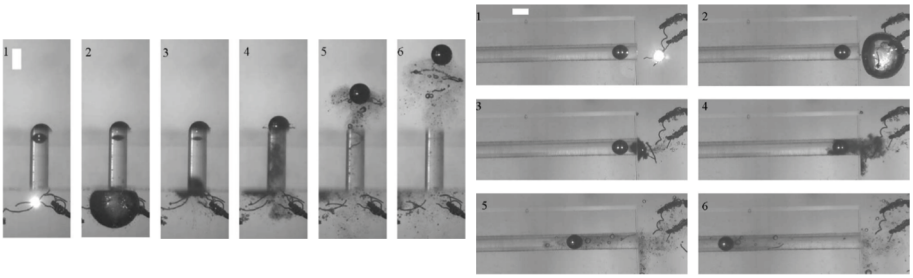

(a) Particle located on a transparent plate (b) Particle located on a horizontal hole underwater

Fig. 12. Process of the collapsing bubble pushing the particles [116].

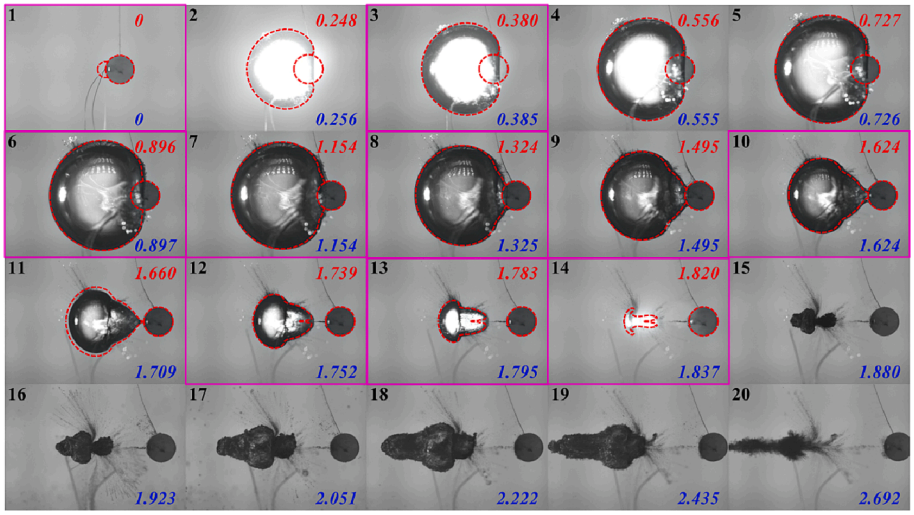

Fig. 13. Motion of particles during bubble evolution [17].

[118]. This could offer an alternative explanation for the failure mechanism of synergistic effects; that is, when the sediment concentration is constant, the damage caused by small particles is less severe.

3.5. Decomposition damage of bubble to particles

When a bubble collapses, it generates an instantaneous local high pressure, resulting in the formation of a shock wave and a micro-jet with a velocity of several hundred meters per second. The high velocity micro-jet has an erosive effect on fine particles [119], leading to the expansion of micro-cracks within particles, acceleration of particle movement, and severe collisions between particles and near-wall surfaces. Moreover, this phenomenon can also result in the fragmentation of brittle particles [120].

Initially, the disintegration of aggregates was believed to occur during the approach of collapsing bubbles [121], but this was not widely recognized due to the lack of visualization. Subsequently, Wagterveld et al. [113] utilized high-speed photography to visualize the effects of acoustic cavitation on various sizes of suspended calcite crystals, and discovered that the cavitation group could lead to abrasion, destruction of aggregation, and disintegration. While flow cavitation leads to deagglomeration, acoustic cavitation destroys the single crystal structure [122], resulting in multiple fragments. In Wang's study [123], it was found that cavitation bubbles or bubble clouds promote fragmentation not only by mechanically fracturing dendrites but also by facilitating the effects of acoustic streaming flow on dendrites. By comparing the behavior of particle dispersion under ultrasonic irradiation and mechanical stirring, Sumitomo et al. [124] determined that ultrasonic irradiation leads to particle splitting by inducing surface cavitation of clusters, and the splitting efficiency is higher than that of mechanical stirring.

The crushing strength of particles exhibits a "size effect," wherein the crushing strength increases with decreasing particle size [125]. In a cavitation jet flow, the micro-particles experience a higher velocity due to the micro-jet produced by the bubble collapse near the wall, thereby increasing the probability of wall impact and particle breakage. According to Rogin's crushing hypothesis, when the kinetic energy at the moment of impact is greater than or equal to the required crushing energy for particle breakage, particle breakage is considered to occur. Zhu [126] derived the dynamic equation governing the impact of bubble collapse on micro-particles in liquid and discussed the effects of dimensionless distance, maximum bubble radius, and particle mass concentration on micro-jet effective particle fragmentation. Huang [127] theoretically estimated the effective range of micro-jet action on quartz particles, and proposed that the effective range for fine particles with sizes less than 100 μm should be less than 150 μm. It is suggested that particle breakage under cavitation is strongly influenced by the near-wall surface and the velocity of the micro-jet.

3.6. Deformation due to bubble-particle interaction

The interaction between bubbles and particles results in bubble deformation. The non-spherical geometry of bubbles can alter their oscillation characteristics, including collapse strength, bubble length, shedding frequency, and period [128-130]. Additionally, bubble deformation can have a significant impact on cavitation erosion intensity [128,129,131]. Shi [132] discovered that the inclusion of particles leads to a reduction in bubble surface tension, causing it to lose its spherical shape, and the maximum radius of the bubble, as well as its pulsation period, decreases as the particle concentration increases. Furthermore,

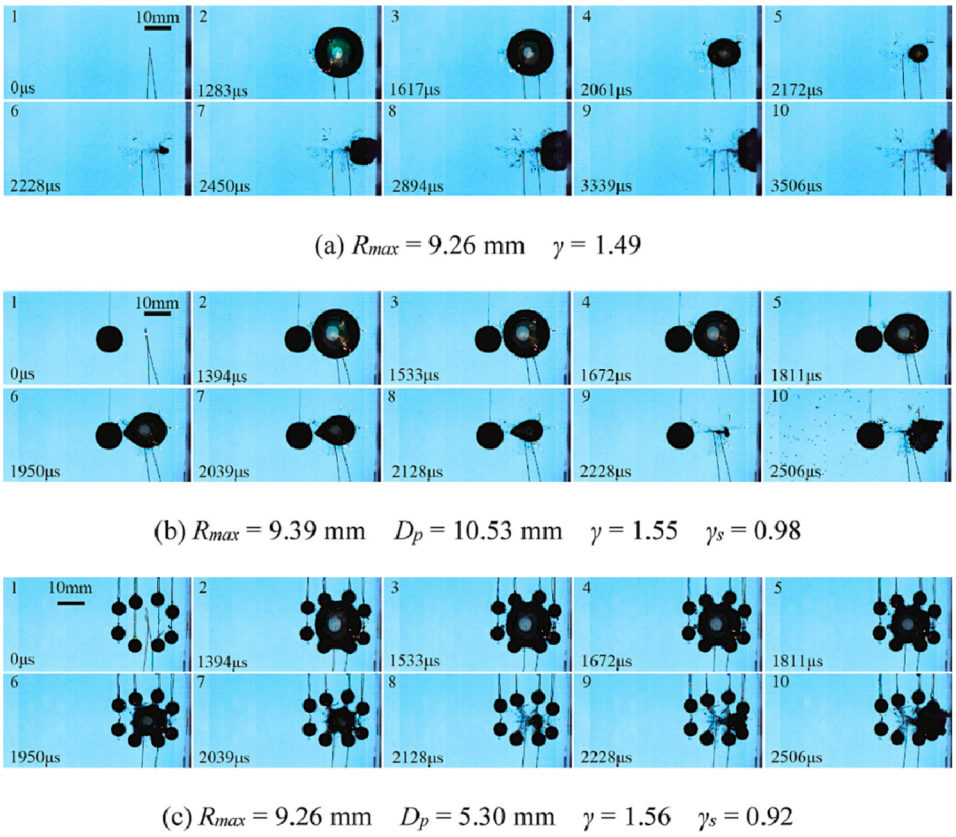

Fig. 14. Effect of particles on the evolutionary morphology of cavitation bubbles. (a) Without particles. (b) The bubble collapses and interacts with a large particle. (c) The bubble collapses and interacts with eight small particles. [118].

Zhang et al. [133] demonstrated, through experimentation, that the presence of particles affects the shape of the bubble during the collapse process and considerably accelerates its collapse. Furthermore, the presence of bubbles can also alter the shape of particles, as illustrated in Fig. 15. At t = 80 μs, the rapid motion of the bubble wall generates a significant amount of tension, which causes particles to deform [134].

3.7. Microscopic mechanisms between bubble-particle

Gas nuclei can be found in the cracks on the surface of rough particles [103], which serve as additional nucleation sites, reducing the water's tensile strength and resulting in a lower cavitation threshold [106,135]. Furthermore, cavitation nucleation also accelerates the attachment of cavitation bubbles [136]. Toshima et al. [41] discovered that the incipient cavitation number of sediment-laden flows is 10%-15% larger than that of clean water. When exposed to external factors that trigger the cavitation threshold (such as a local drop in liquid pressure, a rise in local temperature [137], or a significant increase in liquid tensile stress caused by laser [138] or ultrasound [139,140]), bubbles begin to develop and gradually engulf particles as they grow. Under the influence of the pressure difference, particles acquire kinetic energy and begin to accelerate, moving away from the center of the bubble. Once the growth of the bubble volume begins to slow down, the particles detach from the bubble after necking and continue to move away from it. Afterward, the bubble collapses, and there is a secondary expansion. During this process, particles are likely to undergo secondary acceleration. Finally, the particles gradually slow down until they stop due to the hindrance of viscous forces. If there are other gas nuclei in the particle crack, they may be stimulated by external conditions after the particle separates from the first bubble and develop into a new bubble, repeating the entire process.

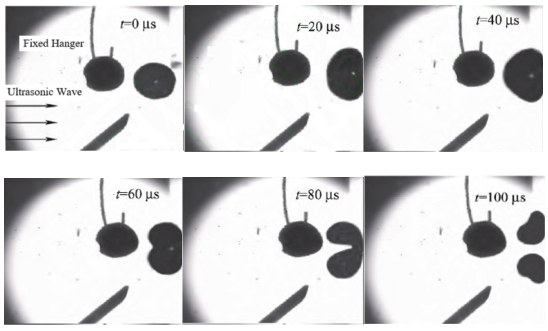

Fig. 15. Deformation of the surrounding particles caused by single bubble collapse [134].

The presence of a gas nucleus near particles heavily influences the particles' motion, which is primarily determined by the initial relative position between the particles and the gas nucleus [141]. This relative position dictates whether the particles can acquire sufficient energy to move and determines the trajectory of the particles.

Particles can gain momentum from the expansion or collapse of bubbles, which can lead to acceleration and impact on the wall. Based on this perspective, the acceleration mechanism of bubbles on particles can be categorized into two types [82] (Fig. 16 provides a description of these two mechanisms): (a) bubble collapse results in particle acceleration, and (b) bubble expansion results in particle acceleration.

Another way to categorize the acceleration mechanism of bubbles on particles is based on micro-jet and shock wave, as depicted in Fig. 17 [126]. (a) Micro-jet induced acceleration involves entrainment of particles by the jet flow, which results in their impact on the material wall [11,98]. (b) Shock-induced acceleration occurs due to the pressure wave induced by bubble collapse, which is regarded as the source of particle

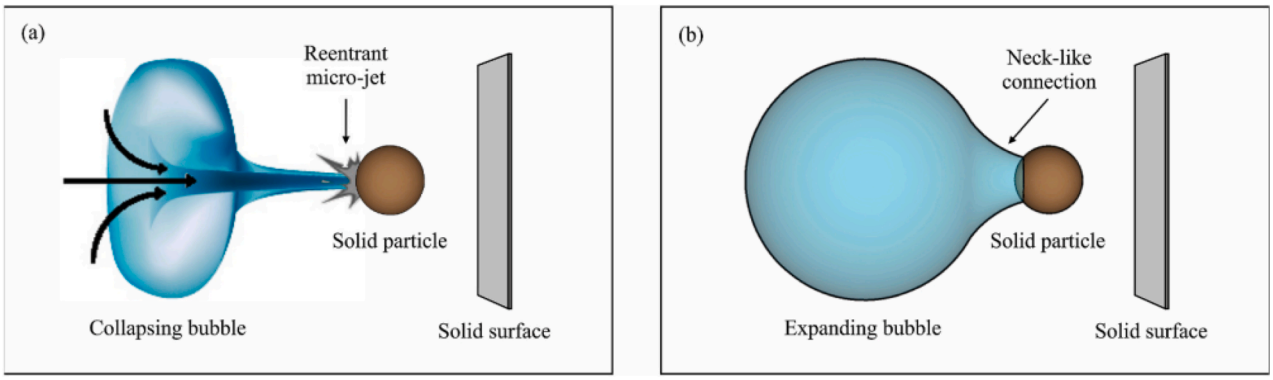

(a)accelerate

Fig. 16. Two acceleration mechanisms of particles [82].

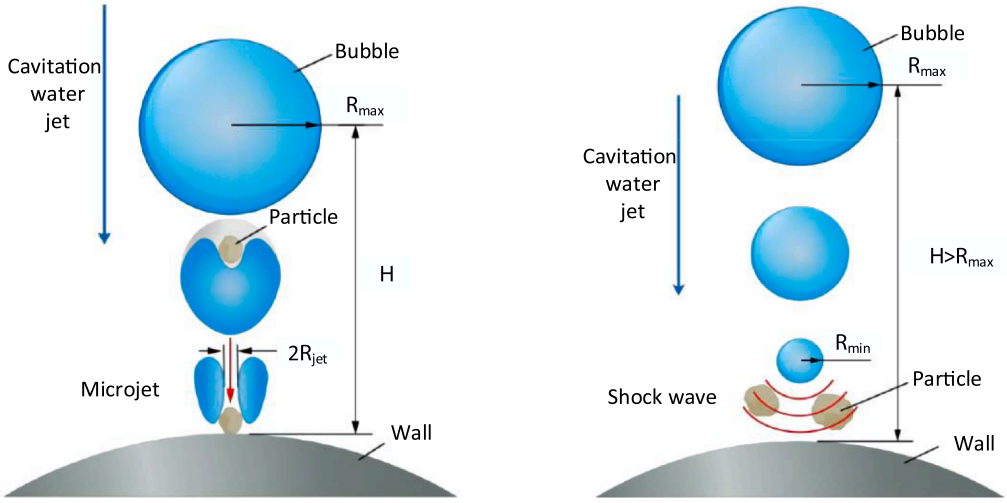

Fig. 17. Acceleration mechanism of particles by micro-jet and shock wave [126].

acceleration [142].

A mechanism for particle acceleration has been proposed that is contingent upon the properties of both micro-jets and shockwaves. The micro-jet and shockwave characteristics are thought to synergistically contribute towards particle acceleration [117]. This is because these two mechanisms may operate concurrently when the pressure wave discharged by the bubble cloud prompts the implosion of local bubbles (refer to Fig. 18).

While high-speed visualization assists in comprehending the microscopic mechanisms of bubble-particle interactions, the majority of studies focus on single or few bubble-particle interactions. In real-world scenarios, there exist tens of thousands of gas nuclei and particles [143],

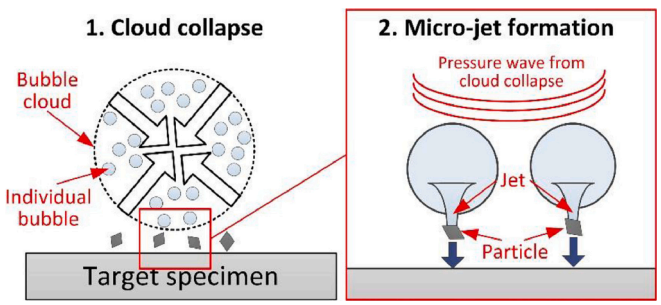

Fig. 18. Particle acceleration mechanism illustration [117].

and erosion is the cumulative effect of the damaging impact on the wall surface due to the interaction of numerous bubble clusters of varying scales and a substantial number of particles. Hence, it is imperative to acquire a better understanding of the macro-level interaction between the two.

4. Bubble-particle interaction at the macroscopic scale

Studying the microscopic mechanisms of bubble-particle interactions can aid in comprehending the dynamics of bubbles and particle motion processes more profoundly [144]. However, practical engineering issues are more concerned with the stripping and destruction of materials caused by the synergistic effect of erosion. In this situation, macroscopic mechanisms are given more consideration and investigation [145].

Unlike microscopic mechanism research methods, macroscopic studies use rotating disks [146-148], slurry pot tests, tunnel tests, Venturi tubes [149,150], and other devices to assess the degree of abrasive damage by observing the mass loss and surface morphology changes of specimens before and after experiments. Although the cavitation erosion mechanism of sand-laden flow has been studied, the results vary, and a consensus is difficult to reach. This is because the complex structure of large hydraulic machinery, operating in an environment mixed with silt impurities, makes the flow characteristics more complex.

In earlier days, it was believed that the damage caused by the

combined wear of cavitation and sediment was much more severe than the sum of the two alone, and several research results supported this conclusion [12,42]. However, with recent research, it has been found that this finding is not always true, and sometimes cavitation can also inhibit or delay sediment erosion. Thus, whether cavitation and sediment wear promote synergistic erosion relies on whether particles can acquire energy from the fluid [11]. Usually, different test conditions result in different wear mechanisms, which involve bubble nucleation theory, bubble dynamics, fluid mechanics, particle mechanics, transient flow of solid suspensions [47], and material mechanics [151].

In the following sections, the interaction between bubbles and particles on a macro scale is discussed from four aspects: (a) promotion and inhibition of the synergy between bubbles and particles; (b) the influence of particle properties on the synergistic effect, including particle size, shape, concentration, and type; (c) the influence of liquid properties on the synergy effect, including liquid viscosity and temperature; and (d) macroscopic mechanisms between bubbles and particles.

4.1. The promotion synergy and inhibition synergy of bubble and particle

4.1.1. The promoting synergistic effect

Cavitation and particle erosion often work together to cause more severe damage to materials [67], as evidenced by numerous studies in the field of hydraulic machinery [45]. Synergistic erosion occurs in two scenarios [45]: firstly, when the surface submerged in water does not have cavitation, but the presence of the stagnation point causes particles hitting the wall at a large angle to peel off material, changing the shape of the component and causing a decrease in local pressure and synergistic erosion. Secondly, when there is cavitation on the surface of the component and sediment is introduced into the flow, the abrasion damage on the flow-passing components is caused by the interaction and mutual promotion of cavitation and sediment wear, resulting in a more significant damaging effect. Experimental results indicate that the damaging effect of abrasion is 8.5 times that of cavitation alone and 3.2 times that of abrasion alone.

Studies have been conducted to investigate the effect of sediment on cavitation erosion in various scenarios. Zhang et al. [152,153] performed a cavitation erosion test on a 120 mm long RAF61 aluminum airfoil with a silt content of 5 g/l, finding that sediment is more likely to cause scratches and impacts on the surface during the bubble growth stage and is more susceptible to the pressure wave during the bubble collapse stage, which impacts the surface at a large angle and accelerates the material damage. Similarly, Gregorc et al. [154] analyzed the influence of particles on the development of cavitation flow conditions around the hydrofoil and found that adding particles increases the depth and degree of cavitation. Lv [155] studied the influence of sediment on the cavitation performance of a hydrofoil at different angles of attack and found that the combined wear was severe at large angles of attack.

Madadnia and Owen [42] conducted a valve device test and found that with only cavitation, the material surface is only discolored; only under the sediment-laden flow some of the material will be removed; when cavitation and sand are present at the same time, there will be substantial material removal. Similarly, Amarendra et al. [156] used a slurry erosion test device to test the synergistic effect of sediment erosion and cavitation and found that the mass removal of materials by the synergistic effect of sediment and cavitation is generally greater than the material loss when sediment erosion alone.

Thapa et al. [157] studied sediment abrasion, cavitation erosion, and synergistic erosion on a rotating disk test rig with cavitation inducers and found that the combined effect on material damage is much greater than the sum of sediment abrasion and cavitation erosion. They also compared the anti-abrasion properties of HVOF sprayed stainless steel and HVOF sprayed WC-CO-Cr and found that the latter is more suitable for the environment of sediment-laden flow. Finally, Peng et al. [36] conducted a submerged cavitating jet flow wear test on a highly accelerated jet test rig and found that the cavitation intensity, noise, and erosion rate were improved after adding silica sand particles. Coarse particles are more likely to induce cavitation, and damage from sharp particles is severe. Additionally, the jet cavitation intensity increases with the increase of micro-particle concentration and decreases with the decrease of micro-particle size.

4.1.2. The inhibiting synergistic effect

Studies have shown that increasing the size and concentration of particles can actually inhibit cavitation damage [158]. This is due to the high energy barrier between particles and gaseous nuclei, which limits the formation of bubbles and prevents destruction of the sample surface by the micro-jet. Other researchers [159] have investigated the combined wear of different particle concentrations and sizes, as depicted in Fig. 19, and found that under certain parameter combinations, the combined wear results in greater material removal than pure cavitation erosion, while in other cases the results are opposite. Huang et al. [160] suggest that although particle size, concentration, and hardness may worsen abrasive wear to a certain extent, they can also alter the physical properties of the liquid mixture, thus reducing the damage caused by cavitation collapse. Together, these factors determine the overall level of erosion.

Su et al. [47] investigated the influence of different sizes and concentrations of sand on cavitation erosion, focusing on both the promotion and inhibition effects. Their observations indicate that small particles (10–50 μm) with increased particle density (>1%) can hinder wear by augmenting the viscosity. Conversely, large particles (50–100 μm) with an increased volume fraction (≤10%) tend to gain more momentum from the bubbles, thereby promoting wear.

Hu et al. [53] conducted a comparative analysis of cavitation and sand-carrying cavitation on 304 stainless steel, and determined that a sediment diameter of 0.152 mm with a 3 wt% concentration represents a critical value. When the concentration is lower than 3 wt%, the sediment restrains cavitation, leading to a decrease in specimen wear. However, when the concentration is greater than 3 wt%, sediment promotes cavitation and enhances the wear of the specimen. The authors attribute the promotion of cavitation wear to the acceleration of sediment by the particle-bubble system during separation and rupture, leading to more severe damage to the specimen's surface. Conversely, sediment inhibits cavitation due to the presence of sediment making the specimen's surface smoother and increasing the flow's viscosity, thus reducing the production of gas nuclei.

Wang et al. [161] examined the impact of micro-particles on the cavitation process using a rotating disk test device with Q235 as the specimen material and disc speed at 2800 rpm. The presence of particles inevitably alters the cavitation erosion process, changing the morphology of the eroded surface, and smaller particles (100 nm, 500 nm) exhibit an inhibitory effect on combined wear. Similarly, Chen et al. [162] demonstrated that adding small particles significantly reduces the cavitation area and volume fraction, with the suppression effect becoming significantly weaker as the particle size increases. Likewise, Gou et al. [163] found through experimental research that increasing the fine particles and turning the liquid into suspension effectively inhibits the occurrence of cavitation in the cavitation-dominated wear process. Conversely, adding large particles aggravates wear.

Since the particle-bubble system exhibits both promoting and inhibiting effects, the study of a single aspect is not sufficient to be scientifically and rigorously comprehensive. Therefore, the present study explores the influence of different factors on the synergistic effect to elucidate the macroscopic mechanism between cavitation and particles.

4.2. The influence of particle properties on the synergistic effect

The occurrence of cavitation erosion in the presence of particles is additionally reliant on various factors, including the impact angle, as well as the shape, size, and hardness of the particles [164,165]. For

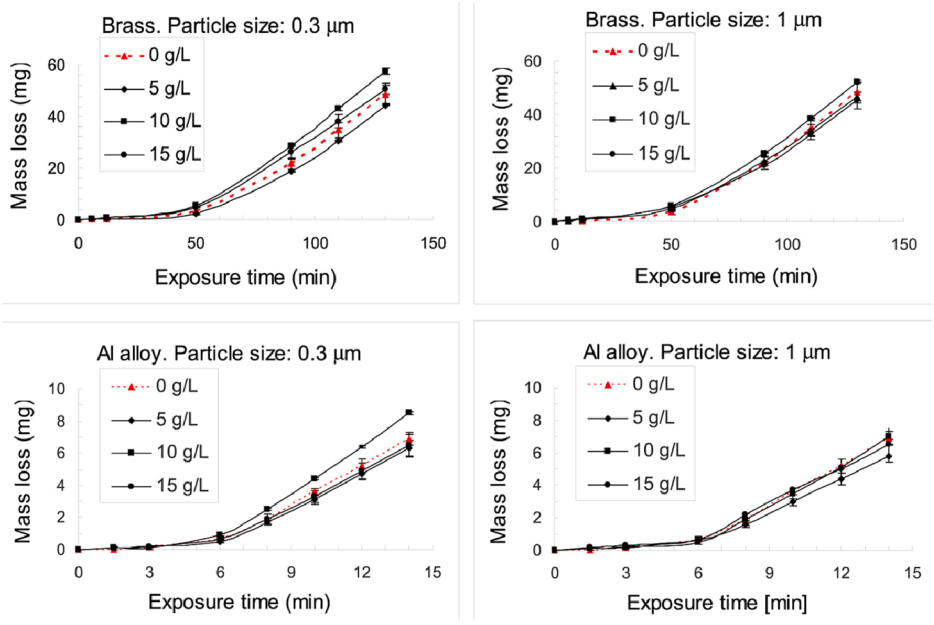

Fig. 19. Curves of mass loss with exposure time, particle size, and concentration [159].

instance, Guo et al. [166] observed that the ultrasonic cavitation effect in magnetorheological polishing fluid (MRPF) is influenced by the properties of solid particles. They found that a high volume fraction of carbonyl iron particles (CIP) considerably weakens the cavitation effect, while a low volume fraction of green silicon carbide (GSC) has only a negligible effect on it. Furthermore, the generation of microjets becomes inconvenient when the liquid viscosity is greater than or equal to 0.1 Pa·s. Hence, it is imperative to investigate the impact of particle properties on the synergistic effect.

4.2.1. *Particle size*

The erosion of walls is greatly influenced by the size of particles. When there is no cavitation, larger particles are predominantly affected by mainstream and secondary flow, while smaller particles are more susceptible to the turbulence structure near the boundary layer. In the presence of cavitation, particles are enveloped by a high-speed jet and impact the wall [11]. The movement of micro-particle bubble union is primarily determined by the particle size, according to Li [167].

The study by Fu et al. [55] shows that micro-abrasive cavitation and synergistic effect are mainly reflected in the shock wave promoting micro-jet formation. Shock waves and micro-jets impart initial velocity to micro-abrasive particles. Within the particle size range of 5 to 50 μm, smaller particles exhibit higher velocity and pressure. Chen's research [168], using SiO2 particles of 500 nm, 2 μm, and 70 μm, investigates the impact of particle size on the cavitation failure of samples. As diameter increases, the number of cavitation pits in samples significantly decreases, and the intensity of cavitation failure gradually lessens. The study of Zhang [169] indicates that reducing particle size in suspension increases the plastic deformation of aluminum alloy surface under cavitation, elevating the surface roughness, and exacerbating the cavitation erosion of aluminum alloy surface. These findings suggest that small particles may increase cavitation failure.

Wu and Gou's study [170] on the combined wear of three sediment concentrations (25 kg/m^3, 50 kg/m^3, and 85 kg/m^3) and five particle diameters (0.531 mm, 0.253 mm, 0.063 mm, 0.042 mm, 0.026 mm) based on a special vibratory apparatus reveals that when the particle size is less than the critical particle diameter of 0.048 mm, the wear effect decreases with the concentration increase; the conclusion is the opposite when the particle diameter is greater than the critical value.

According to Lian et al. [171], the critical particle diameter is about 0.035–0.048 mm. When the sediment particle size is less than the critical size, the damage caused by the combined wear on the material is slightly less than that caused by cavitation under pure water conditions. Gou et al. [172] also tested the combined effects under different conditions and found that the critical particle size at each concentration differed. When the particle size is less than the critical size, cavitation damage is suppressed; otherwise, cavitation damage is promoted. In Liu's study [173], fine particles increase the viscosity of the fluid. The high viscosity of the liquid produces more resistance to bubbles' growth and collapse, reducing the particle velocity, and thus effectively inhibiting cavitation erosion. Conversely, coarse-grained particles do not cause changes in liquid viscosity. In this case, the particles will be accelerated during bubble growth or collapse, aggravating synergistic erosion.

In conclusion, while some studies indicate that the erosion rate increases monotonously with decreasing particle size, the more general conclusion is that there is a critical value for the effect of particles on the synergistic effect. Cavitation erosion is inhibited when the particle size is below the critical value, and promoted otherwise [50,160,161,170]. Table 1 lists the critical particle diameter/concentration under different experimental devices and conditions. When the particle size does not exceed the critical value, the flow contains medium sand and clay with non-Newtonian fluid characteristics, and the flocculation structure formed by the interaction of these particles significantly increases the viscosity of the liquid, alleviating the damage caused by cavitation [174]. However, when the particle size is large, it is difficult to affect the change of liquid viscosity, so collision erosion plays a major role in the synergistic effect, resulting in greater damage.

4.2.2. *Particle shape*

The morphology of particles primarily affects the strength of the material under damage, which is a critical parameter. Particles of varying shapes exhibit differences in the process of material removal [175,176]. However, evaluating particle shapes in natural settings is often challenging. Angular particles create sharp craters, whereas spherical particles generate shallow, more rounded craters [177]. Wear increases as the shape factor decreases and the density increases. Angular particles, when compared to circular and block particles, result in rougher material surfaces and deeper pits during synergistic erosion [49,178].

According to Harvey's theory [179], apart from size, the shape and

Table 1
Critical particle parameters under different experiments.

Testing apparatus	Materials	Experimental Particle parameters	Critical particle parameters	Ref.
Special vibratory apparatus	AMST 1045 carbon steel	25–85 kg/m^3; 0.026–0.531 mm	0.048 mm	[170]
Magnetostrictive-induced cavitation facility	304 stainless steel	0.5–10 wt%	3 wt%	[53]
Vibration cavitation apparatus	40Cr steel	0.1–1.2 μm	0.5 μm	[50]
Rotating-disk testing machine	Q235	0.1–4 μm	1 μm	[161]
Magnetostrictive-induced cavitation instrument	Carbon steel	0.01–0.1 mm; 6–300 kg/m^3	0.04 mm; 30 kg/m^3	[163]
High-pressure water-jet machine	Sandstone	0.075–0.425 mm; 0.56–3.05 wt%	/	[36]
Ultrasonic CEP tests	AISI 1045 carbon steel	10–100 μm; 0.5–20 vol%	50 μm	[47]
Vibratory device	AISI 316 stainless steel	3–10%; 106–150 μm, <53 μm	/	[184]
Vibratory apparatus and custom-made particle-moving device	ASTM 1045 carbon steel	25–85 kg/m^3;0.026–0.531 mm	0.035–0.048 mm	[171]
Ultrasonic cavitation erosion equipment	Ti6Al4V alloy	1–10 mg/L;0.3–23.34 μm	/	[158]
Vibratory apparatus and particle-moving device	ASTM 1045 carbon steel	0.01–0.10 mm;30–150 kg/m^3	0.050–0.058 mm	[172]
Cavitation-slit erosion apparatus	AISI 1045; Carbon steel	0.023–0.249 mm;10–80 kg/m^3	/	[174]
Ultrasonic cavitation erosion tests	Alpha-brass; Aluminum alloy	5–15 g/L;0.3–1 μm	/	[159]
Rotary wear test rig	Q235, 45#, 40Cr, HT200	0.2 mm;1.29 kg/m^3	/	[208]
Cavitation tunnel	Metal	0.1–0.32%;25–35 μm	/	[154]
Ultrasonic vibration cavitation apparatus	6063 Al	0.0018–0.6601 mm;1–85 kg/m^3	0.12 mm	[118]
Venturi tube	Stainless steel	0.023–0.063 mm;25–75 kg/m^3	0.04 mm;50 kg/m^3	[149]

surface profile of particles also influence bubble formation. Bubble growth occurs on smooth and rough spherical particles, but the impact of particle shape on nucleation is yet to be fully comprehended. Chen et al. [49] performed vibration cavitation erosion experiments on particle suspensions with different shapes, namely spherical SiO_2 particles and irregular SiO_2 particles, respectively. The average diameter of spherical particles was 5.0 ± 0.5 μm. They discovered that although irregular particles increased cavitation erosion and particle wear on the surface, the impact of shape on combined wear is significantly less crucial than that of size. However, it should be noted that for irregular particles, additional abrasive effects must be considered during cavitation erosion when determining mass loss rates or analyzing fatigue processes.

4.2.3. Particle concentration

When sand is present in the flow, the critical value of cavitation pressure increases in proportion to the concentration of sediment particles. Zhu et al. [180] suggest that sediment concentration and critical cavitation number are linearly related, with an increase in particle concentration more likely to result in cavitation. This is due to the presence of numerous gas nuclei of varying sizes within the cracks on the surface of particles, whereby increasing the particle concentration will in turn augment the quantity of gas nuclei in the flow [12]. Based on estimates, when the sediment concentration within the water is approximately 8 kg/m^3, assuming a particle size of 0.02 mm and 10 gas nuclei deposited on the surface of each particle, the sediment concentration within the water is approximately 7 million times greater than that found in clear water [101].

Certain studies have shown that an increase in particle concentration can lead to combined erosion. Hong [181], for instance, investigated the impact of particle concentrations of 20 kg/m^3 and 40 kg/m^3 on the combined effect of HVOF sprayed Cr3C2-NiCr coatings on rotating discs, and observed that the wear rate increased with the rise in sediment concentration. Similarly, Xu et al. [182] conducted experimental research on the cavitation properties of deep-sea slurry pumps with varying particle sizes and concentrations. It was observed that as the particle concentration rose from 4% to 10%, the phenomenon of pump cavitation became more pronounced, with the vapor phase volume fraction at the inlet of the first stage front impeller blade considerably enhanced, reaching a maximum of 0.9.

Contrarily, other studies have found that an increase in particle concentration can have an inhibitory effect on combined erosion [174]. Stoian et al. [183], for example, examined the effect of particle concentration (ranging from 0.01 to 0.5 v/v) on cavitation activity in a mechanically stirred solid–liquid container through ultrasonic irradiation. It was noted that as particle concentration increased, the inhibition of cavitation activity grew stronger. This observation was attributed to an increase in apparent viscosity of the suspension caused by the rising concentration, leading to the merging of cavitation bubbles.

However, some studies have contradicted the notion that the increase of particle concentration has a monotonic promotion or inhibition effect on combined erosion, instead suggesting the existence of a critical particle concentration. On the one hand, when the particle diameter is fixed, combined wear initially decreases and then increases with the increase of concentration. Hu [53], for example, studied the combined wear of 304 stainless steel at concentrations ranging from 0.5 wt% to 10 wt% (with an average particle diameter of 0.152 mm) using a magnetostrictive-induced cavitation facility. Results showed that the mass loss of the specimen initially decreased and then increased with the increase of sediment concentration, with the critical concentration being 3 wt%. Similarly, Luo [149] studied the abrasion law of concentrations ranging from 25 kg/m^3 to 75 kg/m^3 and observed a similar trend of decreasing abrasion followed by an increase with the increase of concentration. On the other hand, when particle size varies, the effect of concentration on combined wear differs. Romero et al. [184] tested the combined wear of three different sediment concentrations (3%, 5%, and 10%) for six hours and observed that wear increased proportionally with concentration for larger particles (106 ~ 150 μm), while small particles (less than53 μm) resulted in significantly inhibited combined wear relative to pure cavitation damage. Su et al. [185] studied the cavitation erosion of AISI 1045 carbon steel by SiO_2 particles suspended in oil at different concentrations (ranging from 0.005 v/v to 0.2 v/v) and particle sizes (10 μm, 25 μm, 60 μm, 85 μm, and 100 μm) and found that material removal was more severe at low concentrations and lighter at high concentrations. Large particles aggravated erosion at medium concentrations, whereas small particles reduced erosion.

To conclude, studies investigating the impact of particle concentration on combined wear have yielded seemingly contradictory results. Some studies have suggested that an increase in sediment concentration will result in a reduction in the level of cavitation erosion, while others

have reported an increase in the level of cavitation erosion with an increase in sediment concentration. Conversely, some studies have revealed that the critical concentration, i.e., the concentration before and after the critical concentration on the joint wear effect, exhibit opposite trends. The concentration has a dual impact, with one effect being on the viscosity and the other on the number of cavitation nucleations, and the two mechanisms play opposing roles. Fig. 20 illustrates the wear mechanism of cavitation damage alone and combined action under varying sediment concentrations. The mechanism can be summarized in three main points: (a) Cavitation damage alone, and waveguide effect can lead to large and deep craters. (b) The combined action of a small amount of sediment and cavitation leads to a synergistic wear region and a cavitation-dominated wear region, which exhibit significantly different wear patterns. (c) Under the combined action of a large amount of sediment and cavitation, sediment wear becomes the primary reason for material removal.

4.2.4. Particle type

Yan et al. [186] conducted a study using different types of particles (SiC, AlO_3, and Al) to investigate the synergy effect. The study revealed that the type of particle used had an impact on the acceleration or inhibition of the micro-jet on the damage caused. Among the three particles, aluminum particles demonstrated the greatest potential to minimize the synergistic effect. Similarly, Chen [168] examined the effect of particles on ultrasonic cavitation erosion using four types of micro-particles, namely, SiC, Al_2O_3, Al, and SiO_2. The number of pits on the samples with SiC, Al_2O_3, and SiO_2 micro-particles was significantly higher than that without micro-particles. Notably, the cavitation damage degree of the sample surface with SiO_2 micro-particles was the most severe. On the contrary, adding aluminum particles reduced the number of cavitation pits and inhibited cavitation failure. This phenomenon may be attributed to the unique physical and chemical properties of the Al particle surfaces. Hence, certain micro-particles may have the ability to hinder erosion via cavitation, which is highly significant for anti-cavitation wear studies.

4.3. The influence of fluid properties on the synergistic effect.

The physical characteristics of the liquid can significantly influence cavitation erosion [187], and these factors also play a crucial role in combined wear. As discussed below, fluid viscosity and temperature are relatively critical factors in combined wear.

4.3.1. Liquid viscosity

In 1975, Ashworth and Procter [188] demonstrated the potential of adding polypropylene to water to increase the viscosity of the solution and alleviate cavitation erosion damage. Since then, considerable attention has been devoted to understanding the impact of the appearance of particles or bubbles on liquid viscosity [189,190] and their role in cavitation erosion and combined wear. In general, viscosity refers to the internal friction force in liquid, which is a crucial factor influencing the formation and collapse of cavitation bubbles. By altering the temperature or concentration of the liquid, the mechanism and intensity of erosion can be influenced through changes in viscosity [191]. Additionally, the viscosity of the liquid is generally believed to increase as solid particles are introduced, and researchers have investigated the functional relationship between the two [192,193].

Huang et al. [194,195] have investigated the bubble collapse process and observed that increasing viscosity reduces bubble expansion and prolongs bubble duration. The primary mechanism of cavitation erosion is the interaction between shock waves, micro-jets generated by bubble collapse, and solid boundaries. Therefore, increasing viscosity can reduce the intensity of cavitation erosion by attenuating the micro-jets and shock waves. Similarly, Luo [149] has found that increasing viscosity shortens the length of bubbles and inhibits erosion to a certain extent.

Wang et al. [174] developed a multiple linear regression equation to predict viscosity, taking into account the effects of particle size, concentration, and mixture temperature. They found that viscosity was directly proportional to particle concentration, but inversely proportional to particle size and temperature. Truby et al. [196] investigated the change in relative viscosity of solutions with different initial particle concentrations after adding bubbles. They found that adding bubbles increased the suspension viscosity of diluted particle suspension, but reduced the viscosity for more concentrated particle suspensions. Chen et al. [118] conducted experiments to investigate the effect of particle size on mixture viscosity. They found that when particle size was small ($D_{50} < 0.0804$ mm), the mixture viscosity increased with an increase in particle concentration. However, when the particle size was large ($D_{50} > 0.1583$ mm), the mixture's viscosity was not sensitive to the sediment content, and the viscosity change was less than 5% compared to pure water.

In addition to the inherent physical characteristics of the liquid, the size and concentration of particles also exert a notable influence on viscosity, thereby impacting combined erosion. Nonetheless, the precise correlation and significance of various parameters governing viscosity remain inadequately comprehended and require further investigation.

4.3.2. Liquid temperature

Liquid temperature is also a significant factor in synergistic wear, but this aspect has received relatively little research attention. Wang et al. [174] conducted experimental investigations into the influence of variations in suspension parameters on the synergistic effect at temperatures ranging from 10 to 50 ℃ and found that the wear rate increased with increasing temperature. One possible explanation for this trend is that the temperature increase results in a reduction of liquid viscosity, thereby promoting combined wear. The relationship between viscosity and temperature can be mathematically expressed as follows:

$$\mu = 1.07c^{3.56}\cdot d^{-1.93}\cdot T^{0.88} + 1.13 \quad (1)$$

where c represents particle concentration, 10 kg/m^3 $\leqslant c \leqslant$ 80 kg/m^3.d is particle size, 0.023 mm $\leqslant d \leqslant$ 0.046 mm. T is liquid temperature, 10 ℃$\leq$ T $\leq$ 50 ℃。

In addition to the temperature of the liquid, the temperature of the particles also has a significant impact on cavitation. Research has shown that increasing the surface temperature of the particles from 40 °C to 99.9 °C promotes the development of cavitation. When Re > 200, the

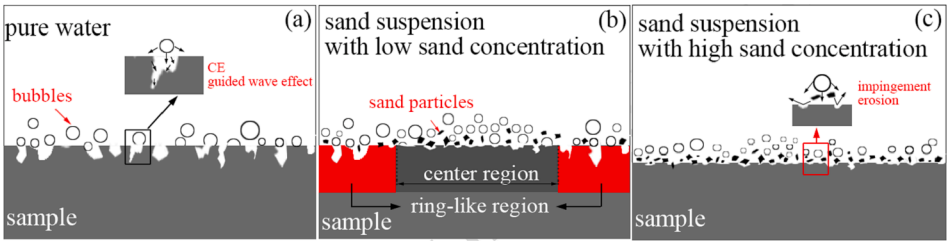

Fig. 20. Wear mechanism of cavitation alone and synergistic effect at different sediment concentrations [53].

average vapor production increases by 200% [197].

4.4. Macroscopic mechanisms between bubble and particle

Due to the complexity of the macroscopic mechanism, it is helpful to explain the synergistic wear phenomenon from two different perspectives: the generation and coalescence of free bubbles in the particle-bubble system and the contest between viscous and inertial forces in the particle-bubble system.

4.4.1. Generation and coalescence of free bubbles in the particle-bubble system

When sediment is added to the water, the effect on the gas nucleus can be expressed in the following equation [50]

$$N_a = N_m + N_t - N_c \tag{2}$$

Where, N_a is the total number of bubbles; N_m is the number of bubbles from homogeneous nucleation, mostly from gas nuclei in the liquid; N_t is the number of bubbles from heterogeneous nucleation, mostly from gas nuclei in particle cracks; N_c is the number of bubbles bound to particles by collisions, which reduces the number of free bubbles. Particle-bubble collision is a predominant mechanism for particle-bubble interactions, governed by the dynamic behavior of particles in the hydrodynamic field surrounding bubbles [198]. The frequency of collisions and agglomeration events between bubbles and particles is influenced by the size of the particles [199] and the hydrodynamic forces generated by the aqueous medium [200]. The flotation theory proposes that particles adhere to small bubbles due to the surface tension of the liquid, causing the particles to be separated from the bulk liquid [201,202]. Accordingly, the expression is given as follows.

$$n = 3k\pi RrVN_0 \tag{3}$$

Where, k is a factor ; R is the radius of the ellipsoid perpendicular to the axis of motion, r is the particle radius, V is the velocity of the bubble relative to the particles, and N_0 is the number of particles per unit volume.

When the particle size is too small, particle agglomeration can reduce the number of free bubbles. Conversely, larger particles can increase the number of collisions between particles and bubbles, ultimately reducing the number of free bubbles. As a result, the value of can only be minimized when the particle size reaches an optimal value, which may explain why the impact of particle size on synergistic erosion reaches a peak at a certain point. However, the mechanism of combined wear is multifaceted and intricate, and this is only one aspect of it.

4.4.2. Conflict of viscous and inertial forces within the particle bubble system.

The phenomenon of double inhibition or promotion of particles in the combined action of the particle bubble system can be explained as a competition between the viscous and inertial forces [82]. When the viscous force dominates, the particles exhibit a more viscous effect, whereas the impact of the particles becomes dominant when the inertial force takes over. Accordingly, this synergy mechanism can be elucidated based on the prospects of promotion and inhibition.

The main reasons for the synergistic effect of erosion promotion are:

(a) According to the heterogeneous nucleation theory [203], the addition of particles to water significantly reduces the surface tension required for cavitation. Adding 76 particles during the experiment can decrease the liquid pressure by one-third [105], thus being more conducive to stimulating cavitation.
(b) The presence of particles increases the number of gas nuclei and bubbles [12].
(c) The occurrence of cavitation significantly alters the original flow pattern, leading to more violent and complex flow structures [204,205], such as periodic cavity shedding accompanied by strong vortices [41], which enhances the destruction potential of particles.
(d) Cavitation accelerates the impact of particles during expansion and collapse, thereby increasing the wear of particles on the material surface.
(e) The presence of particles modifies the pressure distribution, which can expand cavitation. Additionally, the combination of particles and bubbles in the flow generates a region of high pressure, causing the collapse of the bubble [161].

The main reasons for the synergistic effect of erosion inhibition are:

(a) Particle erosion smoothens the surface and reduces the number of gas nuclei on it [206].
(b) Particles prevent further damage to craters caused by shock waves by flattening the edges of craters that arise from cavitation [53]. This can be verified by comparing the surface roughness of the specimens. The surface roughness after combined wear is typically lower than that observed under cavitation alone [53].
(c) The addition of particles can increase fluid viscosity and inhibit bubble growth, thus reducing cavitation erosion [50,207].

5. Model of synergetic effects

5.1. Development of synergistic effect model

Initially, wear models relied heavily on empirical or semi-empirical formulas that were derived from extensive testing or statistical models [209,210]. Gou et al. [172] conducted 74 independent experiments to study the impact of sediment on cavitation and material damage and established a combined damage model in three steps: (a) establishing a model between damage and sediment, (b) establishing a model between silt-laden river and damage, and (c) proposing a standard model of hydraulic mechanical damage evaluation. However, the formula coefficients based on experiments are not universally applicable.

Over time, erosion wear [211] and abrasive wear [212] models have been extensively studied and refined. The loose coupling model [103,213,214] and the full coupling model [215,216] have been widely used to describe the interaction between bubbles and structures. Potential flow, viscosity, and compression models have been shown to better describe the flow field generated by bubbles [217]. Georges et al. [218] combined the boundary element method and the compressible finite difference method to simulate fluid/structure interaction by coupling bubble dynamics with finite element structural models. This allowed for the effective and accurate capture of non-spherical bubble dynamics and fluid pressure, as well as the study of material deformation and pitting during bubble collapse by utilizing fluid and material dynamics and their interaction.

On the other hand, bubble-particle interaction is a transient problem of fluid-structural interaction (FSI), which is highly complex. Currently, all numerical studies on the interaction between bubbles and spheres use potential flow theory and boundary element theory. Although a widely accepted synergistic erosion model has yet to emerge, several models still need to be explored to better understand the bubble-particle mechanism. Here, we describe several typical models of bubble-particle interaction.

5.2. Several typical models of synergistic effect

5.2.1. Li model and Dunstan model

Li [45] was the first to develop a bubble-particle combined model, which could be utilized to uncover the promoting mechanism of cavitation on sediment erosion. The micro-jet generated by the collapse of the bubble near the wall causes particles to gain high velocity and impact the wall, leading to material damage. The model is based on three assumptions: (a) when the bubble collapses, it captures particles

and places them in the center of the jet; (b) the particle will be accelerated to a very high speed; (c) after the particle rotates, its sharp edge aligns with the material. In the Li model, the relative inertia m^* and relative stiffness k^* formulas are established to aid in the calculation of bubble-boundary interaction under the three different types of boundaries, which are represented as follows:

$$m^* = \frac{m}{\rho R_{\max^3}} \tag{4}$$

$$k^* = \frac{k}{(p_\infty - p_c)R_{\max}} \tag{5}$$

where, m is the mass of boundary surface (coating) corresponding to the maximum bubble diameter; ρ is the water density; $R_{\max}$ is the maximum bubble radius; k is the spring constant of the boundary surface (coating); p_∞ is the pressure in the water infinite; p_c is the saturation vapor pressure of the water. For a rigid boundary ($m^*\to\infty$ and $k^*\to\infty$); for a free surface ($m^*\to 0$ and $k^*\to 0$).

Li's model provides a potential explanation for the different wear effects experienced by different wall positions in the same environment [219]. However, the model only offers a general explanation of the interaction between the particle and the bubble and does not provide a detailed account of the underlying mechanism.

Dunstan [11] developed a 2D simplified model based on the Li model [45] to simulate the process of particles obtaining energy from the collapsing bubble. The Dunstan model serves as a further development and complement to the Li model, offering insights into the synergistic mechanism. To portray the behavior of particles, Dunstan employed translational and rotational motions. The model assumes that particles exhibit two degrees of translational freedom and one degree of rotational freedom. Equations (6) and (7) present the translational and rotational equations, respectively.

$$\begin{cases} F_x = m_p \dfrac{dv_x}{dt} \\ F_y = m_p \dfrac{dv_y}{dt} \end{cases} \tag{6}$$

$$\begin{cases} T_1 = 0.25b\left(1 - e^{3(1-\beta)}\right)\left|\cos^3\alpha\right| \times \left(\vec{F}_L + \vec{F}_D + \vec{F}_{VM} + \vec{F}_{PG}\right) \\ T_2 = \dfrac{1}{64} C_D \rho_L \omega_p^2 D L^4 \end{cases} \tag{7}$$

where the subscripts $\times$, y refer to the two dimensions, v is the particle velocity, F is the sum of the forces acting on the particle and m_p is the particle's mass. T_1 and T_2 are the hydrodynamic torque acting on the particles to rotate them. $\vec{F}_D$ is the drag force upon the particle. $\vec{F}_L$ is the lift force acting on the particle. $\vec{F}_{PG}$ is the force due to a pressure gradient. $\vec{F}_{VM}$ is a force due to the virtual mass. β is the particle aspect ratio. α a is the angle of attack. C_D is the drag coefficient. ρ_L is the density of the fluid. L is the particle length and D is the height of the projected face at each point along the length L.

The model established by Dunstan [11] not only confirmed that the particles in the Li model would be accelerated by the microjet of bubble bursting, but also verified the numerical model by Star CCM$^+$ and MATLAB. The model suggests that the synergistic erosion enhancement is primarily affected by particle mass and the ratio between the distance of bubble-boundary and the collapse radius during bubble collapse. However, due to the two-dimensional nature of the numerical simulation, it has limitations when applied to practical problems.

5.2.2. Wu model and Borkent model

Wu et al. [114] carried out experiments to investigate the behavior between laser-induced bubbles and free-settling particles and proposed a particle-bubble dynamic model. The model was established based on three assumptions: (a) neglecting the gravitational sedimentation of the particle during the particle-bubble interaction time; (b) ignoring the influence of the particle on the flow field around the bubble; (c) assuming one-dimensional motions of the bubble and the particle. The model results were compared with experimental results to verify the accuracy and reliability of the model, as illustrated in Fig. 21. This model offers an effective explanation for the erosion failure enhancement mechanism in silt-laden flow, and has a more precise mathematical description of the particle-bubble interaction, which is a significant improvement over previous models. However, the effect of particles on the cavitation dynamics is not considered in the model, and the impact of bubbles and particles being too close on the non-spherical characteristics of bubbles is disregarded. A fully coupled particle bubble model is necessary to comprehend the physical interaction process.

The particle motion equation is

$$\frac{d^2\lambda}{dT^{*2}} = \frac{\frac{3C_d}{4\gamma}\left|u_f^* - u_p^*\right|\left(u_f^* - u_p^*\right) + 3\frac{Du_f^*}{DT^*}}{\left(1 + 2\frac{\rho_p}{\rho_f}\right)} \tag{8}$$

The bubble dynamics equation is

$$\frac{R}{R_{\max}} = \left[1 - \left(\frac{t}{T_c} - 1\right)^2\right]^{\frac{2}{5}} \tag{9}$$

Where, $T^* = t/T_c; \gamma = a/R_{\max}; \lambda = l/R_{\max}; u_f^* = u_f/(R_{\max}/T_c); u_p^* = u_p/(R_{\max}/T_c); T_c = 0.915 R_{\max}\sqrt{\rho_f/(p_\infty - p_v)}$, T_c is the Rayleigh time of a spherical cavitation bubble; l_0 is separation distance (between the particle center and the bubble center); $R_{\max}$ is maximum bubble radius; a is particle radius; ρ_p is particle density; ρ_f is fluid density; μ_f is fluid viscosity.

Borkent et al. [103] utilized axisymmetric boundary elements to construct a mathematical model of particle-bubble interaction and conducted a simulation using the boundary element method (BEM). The model was established based on potential flow theory and made several assumptions, including the symmetric spherical shape of the bubble and the neglect of surface tension, compressibility of water, and viscous effects during supercritical expansion. Fig. 22 illustrates the comparison between simulation results and experimental records, indicating that the axisymmetric BEM method's calculated bubble shape is consistent with the experiment until the neck is formed. However, the simulation neglects the bubble-particle contact conditions, leading to a slightly different cavity shape compared to the experimental one. Furthermore, there is insufficient understanding of the relationship between particle velocity and maximum bubble size, particle diameter, particle density, and particle shape.

5.2.3. Poulain model Su model

Poulain et al. [84] formulated a model to investigate the effect of spark-induced bubbles on the motion of freely suspended particles, utilizing the theory of asymmetric bubble dynamics based on extensive experimental data. The velocity equation for particle motion and the equation governing the change in bubble radius are expressed as follows:

$$\dot{X}_{p,f} = \frac{\frac{1}{2}C_D \rho_f \pi R_p^2}{X_{p,i}^4 m_{eff}} \left(\int_0^{t_g} R_b^4 \dot{R}_b^2 \, dt - \int_{t_g}^{t_g + t_c} R_b^4 \dot{R}_b^2 \, dt \right) \tag{10}$$

$$\frac{R_b(t)}{R_{b,\max}} = \begin{cases} f\left(\dfrac{t}{t_g}\right) & \text{if } t \in [0; t_g] \\ f\left(\dfrac{t_g + t_c - t}{t_c}\right) & \text{if } t \in [t_g; t_g + t_c] \end{cases} \tag{11}$$

Where $\dot{X}_{p,f}$ is the velocity of particle movement; $X_{p,\,i}$ is the initial distance from the particle to the gas nucleus; t_g, t_c are the duration of

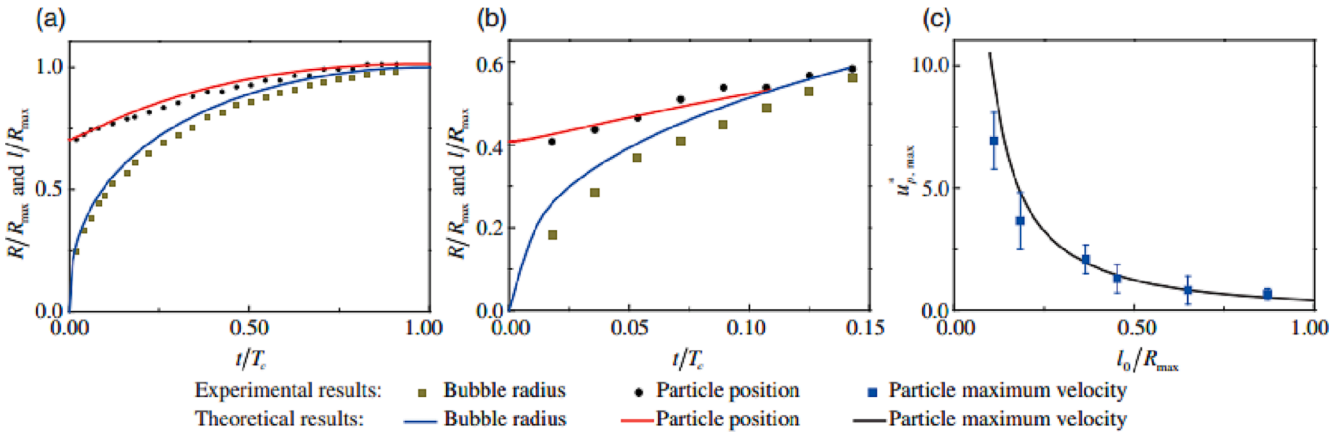

Fig. 21. Comparison of theoretical and experimental values [114].

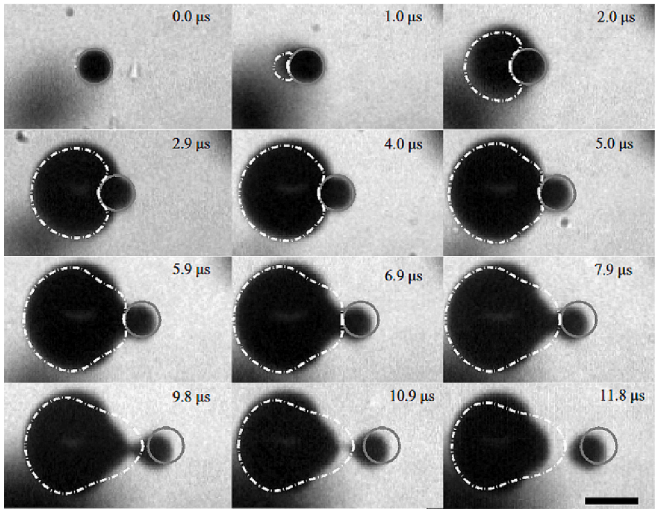

Fig. 22. Comparison between simulation results and experimental records (The contours of the particle and bubble obtained by simulation are represented by solid gray lines and dashed white lines, respectively) [103].

bubble growth and collapse, respectively;$\dot{X}^*_{p,f}$ is the normalized particle velocity,$\dot{X}^*_{p,f} = -\dot{X}_{p,f} \times m_{\text{eff}}\tau/\left(\rho_w R_p^2 R_{b,\max}^2\right)$;$X^*_{p,i}$ is the normalized initial distance,$X^*_{p,i} = X_{p,i}/R_{b,\max}$.

The velocity of the particle exhibits a robust inverse quartic correlation with the distance of the bubble. Fig. 23 depicts the comparison between the empirical findings and the analytical model, which shows that the error is reasonably low. Nevertheless, this model has several limitations, such as: (a) the bubble is spherical, (b) separation parameters$\gamma > 1$,$\gamma = \left(X_{p,i} - R_p\right)/R_{b,\max}$ and (c) this model focuses on the motion of particles after the bubble disappears rather than the motion of particles during the whole development of the bubble.

Su et al. [82] developed a theoretical model to forecast erosion, by taking into account viscous and inertial effects, which arises from the interplay between particles that can either inhibit or promote synergistic effects. The model is established based on three assumptions: (a) In the semi-dilute regime, the second-order term that was ignored in Einstein's equation is considered; (b) The erosion caused by silt-sized particles (STPs) is influenced by modifying the properties of the liquid, hence both the liquid and suspended STPs can be treated as an effective medium in which sand-sized particles (SDPs) are suspended; (c) The liquid and suspended STPs are treated as a continuous phase. The diagram of a bubble-particle system and the volume unit of particle suspension is depicted in Fig. 24. Fig. 24(a) depicts the bubble-particle system during the growth stage of the bubble. SDP is the sand-sized particle. R_b and R_p

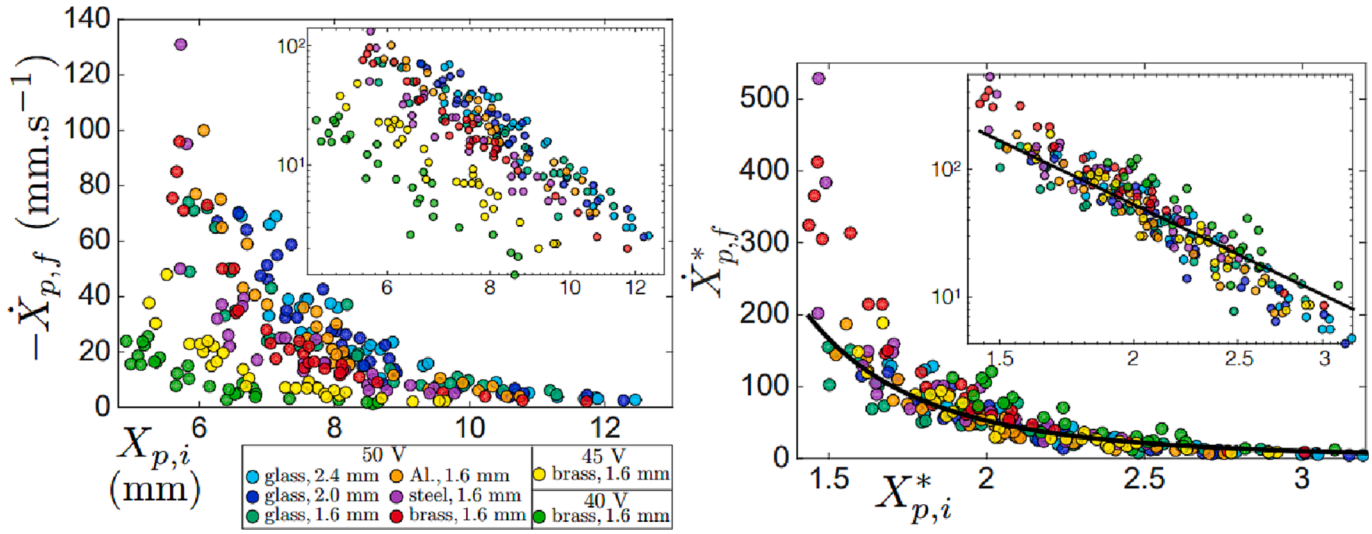

Fig. 23. Comparison between experimental and model [84].

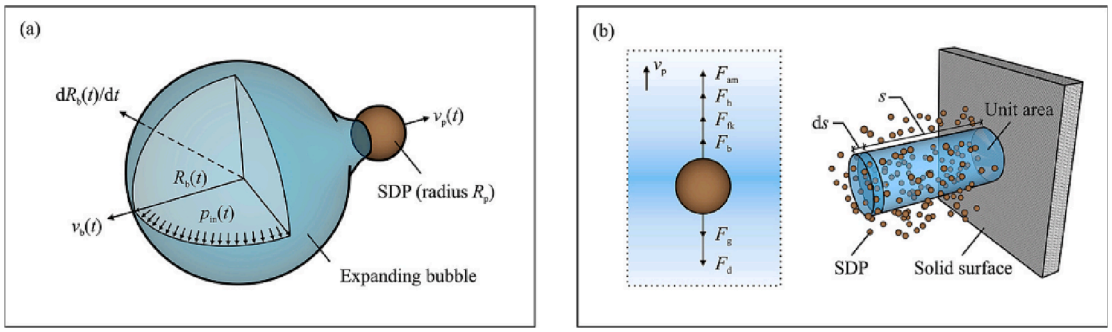

Fig. 24. Diagram of a bubble-particle system and volume element of particle suspension [82].

are the radius of the bubble and SDP, respectively, while v_b and v_p are the velocities of the bubble and SDP, respectively, and their directions are opposite. Fig. 24 (b) describes the volume element of particle suspensions. *ds* is the unit area; *s* is the unit height. The forces on the particles are as follows: Stokes' drag (F_d), Froude–Krylov force (F_{fk}), added mass (F_{am}), Basset force (F_h), gravity (F_g), and buoyancy (F_b). Instead of solely focusing on the acceleration of a single particle through impact as seen in previous research, this model takes into account the collective impact of multiple particles. While the particle impact energy calculated by this model is able to accurately match experimental data, it should be noted that the test sample used is limited and the model does not consider the promoting effects of micro-jets or shock waves on particle impact.

5.3. Develop trends of synergistic erosion modeling

When developing a synergistic erosion model, it is crucial to consider the location where combined erosion may occur. Additionally, the dual role of particles in synergistic effects, which includes the inhibitory effect dominated by viscous forces and the promoting effect induced by particle collisions dominated by inertial forces, must be fully taken into account. Furthermore, when perfecting the model, the impact particles generated by micro-jets or shock waves should also be considered [82]. For irregular particles, an additional abrasive effect should be taken into account when calculating the mass loss rate or analyzing the fatigue process during cavitation erosion.

6. State-of-art numerical simulation of synergistic erosion

The application of numerical simulation technology has facilitated obtaining relatively reliable results at a lower cost and in a more efficient manner. Numerical models for predicting cavitation and sediment wear have witnessed rapid development in recent decades. Presently, the numerical calculation of cavitation in sand-laden flows is mainly based on the coupling calculation of the cavitation and multiphase flow models. However, the interaction between phases is seldom considered, resulting in a lack of accuracy of the results. Developing a numerical model of cavitation and sediment with higher reliability and accuracy is vital for accurately predicting the location and rate of abrasion and achieving the purposeful enhancement of design, processing, inspection, and maintenance of flowing-passed components [220]. In the following sections, advanced numerical simulation techniques of synergistic erosion will be introduced from three perspectives: research progress in numerical simulation, key models selected for numerical simulation, and several challenging issues in numerical simulation.

6.1. Research progress of the numerical simulation

6.1.1. Numerical simulation of a single bubble-particle

Teran et al. [110] utilized the axially symmetric fluid domain geometry to conduct a simplified numerical simulation of the particle-bubble interaction when pressure changes occur near the solid wall. The results are comparable to the experimental data, as illustrated in Fig. 25, although the effects of surface tension and viscosity are not considered in the calculations. Later, Teran et al. [221] established a combined wear model based on simplifying the interaction between spherical particles and bubbles and applied it to CFD simulation. This model can estimate the collision velocity of particles that are trapped by the micro-jet of collapsing bubbles and predict the synergistic effect of cavitation damage and hard particle erosion.

The study conducted by Li et al. [215] utilized the integral boundary method to model the interaction between particles and bubbles. The results showed that numerical simulation could accurately predict various phenomena, such as particle acceleration, bubble shrinkage, mushroom-like bubbles, bubble-particle separation, and the secondary acceleration of particles during the collapse of bubbles. Fig. 26 depicts the process of bubble-particle interaction.

Zevnik and Dular [222] developed a model for the collapse of an unbounded spherical bubble using the FVM-VOF method, considering surface tension, viscous effects, and nonlinear compressibility of water. Their research showed that the mechanical load of spherical particles increased with the increase of the spherical bubble size ratio and decreased with the increase of the spherical bubble spacing, as illustrated in Fig. 27.

6.1.2. Numerical simulation of synergistic effect on hydraulic machinery

In the combined effect studies based on hydraulic mechanical models, external characteristics are used to evaluate the effect of sediment particles on the hydraulic components. While most numerical simulation studies confirm only the promoting effect of particles on synergistic effects, Liao et al. [223] examined the cavitation characteristics of Kaplan turbines under both pure water and solid–liquid two-phase flows. They found that the presence of sediment not only increased the cavitation probability but also caused more severe wear on the runner blades, particularly under conditions of high sediment and large diameter. Compared to clean water, the vapor volume fraction of the pressure and suction sides of the blade in the sand-laden flow increased by 6.9% and 17%, respectively, and the efficiency decreased by 1.68%. Large particles (0.1 mm) resulted in a poor flow pattern, exacerbating the uneven sediment distribution on the blade and leading to a greater erosion rate. Pang et al. [208] conducted a numerical simulation study on a wear test rig and discovered that compared to pure cavitation erosion, the high-pressure region of combined erosion became smaller, the pressure value increased, and the pressure gradient became larger. However, combined erosion was found to be more severe than single cavitation or sand erosion. Liu et al. [224] developed a coupling CFD model to simulate the cavitation erosion and particle erosion of a butterfly valve and validated the numerical model through a flow coefficient experiment. They found that the maximum velocity, mass flow, wall shear stress, turbulence intensity, and particle erosion all increased with increasing inlet pressure and decreased with decreasing valve opening.

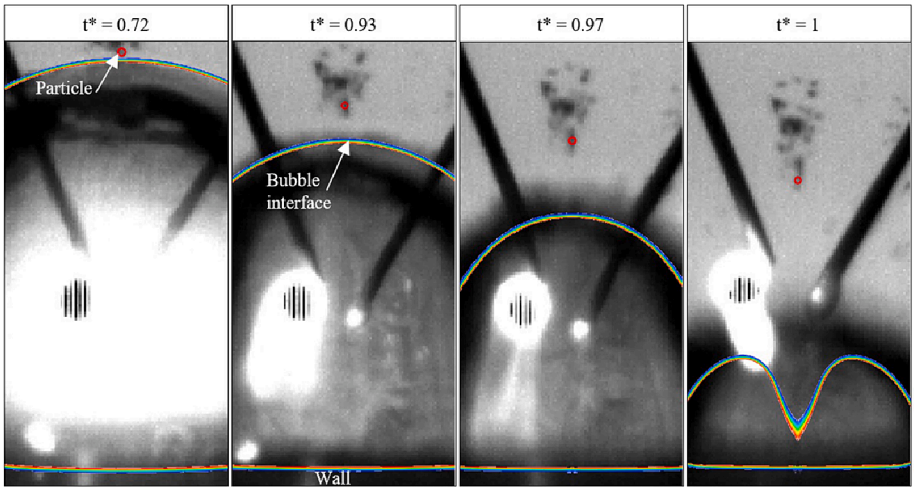

Fig. 25. Comparison between the image sequence obtained by experiment and the bubble interface obtained by CFD simulation [110].

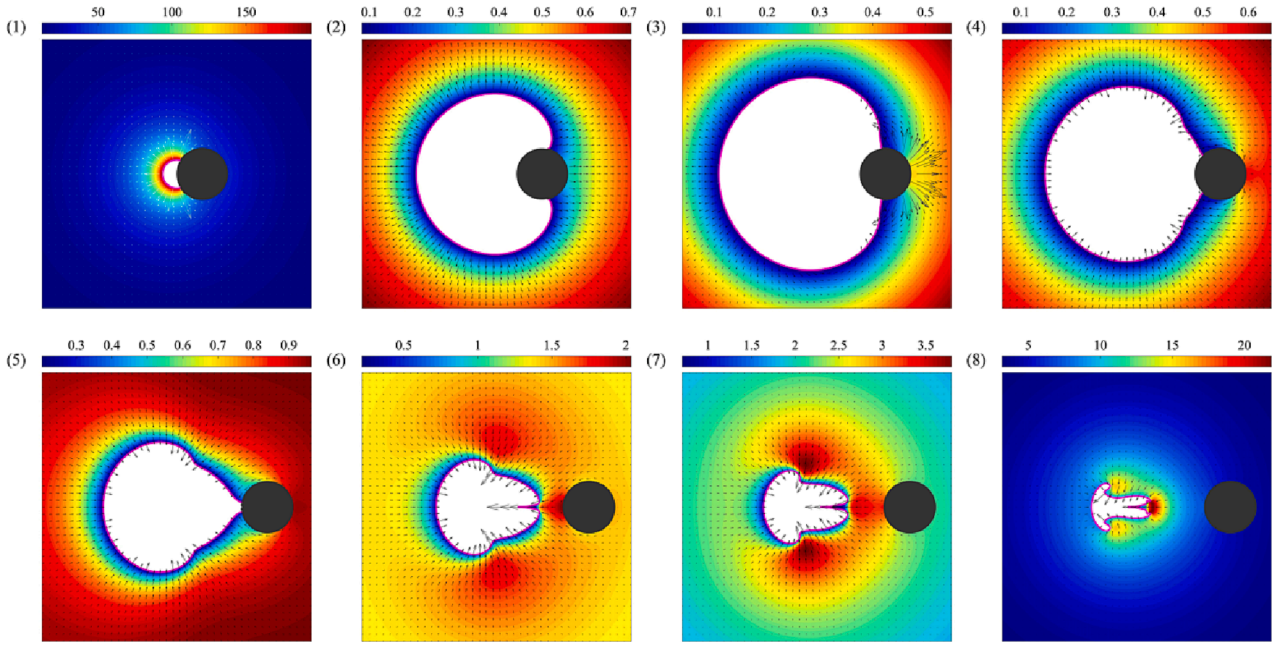

Fig. 26. Bubble-particle interaction process [215].

Kumar et al. [225] conducted numerical simulations to investigate the effects of pure water, cavitation, sediment, and combined erosion conditions on a 7 MW rated capacity Kaplan turbine. The results showed that sediment presence increases the likelihood of cavitation, leading to a 4.3% reduction in maximum efficiency under combined erosion. Additionally, sediment diameter and concentration contributed to increasingly uneven sediment volume fraction distributions on the blade. Lin et al. [226] analyzed the internal flow field of an axial flow pump under different particle sizes and concentrations to examine sediment influence on pump cavitation. Their findings revealed that sand-laden flow cavitation areas were larger than those of clean water. Particle size had little effect on cavitation distribution, while sand content was the primary factor influencing pump cavitation performance. Sediment concentrations also led to vortex and blade cavitation area expansion, as well as chaotic impeller flow patterns. Luo [149] utilized the Eulerian-Lagrangian method to investigate synergistic erosion of the venturi tube, and discussed the influence of particle size, concentration, and liquid viscosity on cavity development (as displayed in Fig. 28). They discovered that these parameters did not significantly affect cavitation shedding frequency, but cavitation presence easily caused re-entrant flow wear. As particle diameter increased, the weight of viscosity on wear decreased (see Fig. 29).

Studies have shown that particles can have paradoxical effects on cavitation, either inhibiting or promoting it. Zhao et al. [227] conducted numerical simulations on centrifugal pumps with different sediment concentrations and particle sizes and evaluated the influence of sediment on cavitation through the critical net positive suction head (NPSH). At a sediment concentration of 1%, the effect of particle size on cavitation was first enhanced and then inhibited. When the particle size was 0.010 mm, the effect of sediment concentration on cavitation showed a tendency towards early promotion and eventual inhibition. Sun et al. [228] used a heterogeneous multiphase flow model and cavitation model to simulate the synergistic effect of a rotating disk under different sediment conditions. They found that increasing particle size first inhibits and then promotes cavitation, and large particle size not only enlarges the cavitation area but also intensifies the cavitation damage. Increasing particle concentration can promote cavitation and enlarge the cavitation area, but has little effect on the intensity of

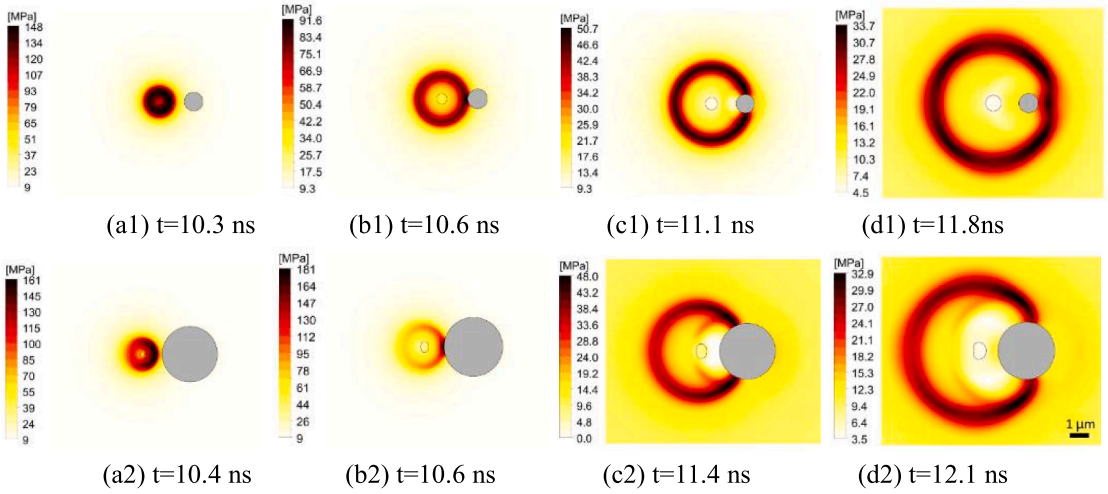

Fig. 27. Pressure field under different bubble size ratios shows the propagation of bubble emission shock wave at different times [222].

Fig. 28. Particle trajectory and cavity structure in Venturi tube [149].

cavitation damage. Zhao et al. [229] also studied the centrifugal pump cavitation characteristics of particles and obtained similar conclusions that particles can have both inhibitory and promoting effects on cavitation under different sediment parameters.

Table 2 serves as a guide for selecting the appropriate research object, parameters, calculation models, and codes for synergistic numerical simulations. Based on Table 2, the typical approach for simulating the synergistic effect on hydraulic machinery involves coupling the multiphase flow, cavitation, and wear models to carry out calculations. The control variable method, which involves manipulating factors such as the size or concentration of particles, is commonly employed to investigate the weight of a specific influence on the synergistic effect. However, it is worth noting that most numerical simulations lack verification with relevant experimental results, thus leading to qualitative rather than quantitative conclusions. To ensure calculation accuracy, proper selection of the turbulence model, multiphase flow model, and cavitation model is crucial. Furthermore, it is important to fully consider the interaction between phases and the impact of particles on the liquid's viscosity. These aspects are explored in greater detail below.

6.2. Several key models selected in numerical simulation

6.2.1. Turbulent model

The selection of an appropriate and precise turbulence model holds great significance in ensuring the accuracy of the results and computations. The standard $k-\omega$ model is commonly employed for low Reynolds number shear flows [232], albeit with evident limitations in dealing with flow separation and reattachment [233]. The $k-\varepsilon$ model has been integrated with the SST $k-\omega$ model to enhance the accuracy of flow separation prediction. In the initial stages of numerical simulation research, the SST $k-\omega$ model was often utilized to solve steady cavitation problems in sediment-laden water flows due to its reliability and precision. However, it cannot simulate the unsteady cavitation process, particularly shedding and collapse, and is thus unsuitable for unsteady calculations [231]. The RNG $k-\varepsilon$ model considers turbulence anisotropy and swirling flow conditions [234], resulting in improved accuracy in dealing with high turbulence at the end of the cavity [235]. Nonetheless, it has been observed that the RNG $k-\varepsilon$ model, regardless of compressibility, encounters issues when calculating cavitation development [236]. Recently, the RNG $k-\varepsilon$ model based on density modification has been proposed to mitigate the effects of viscosity overprediction on the re-entrain jet [237,238], and is considered the most accurate and consistent with actual conditions. All aforementioned models fall under the Reynolds-averaged Navier-Stokes (RANS) model category. Although large eddy simulation (LES) is capable of providing more precise and dependable predictions of flow motion over a particle than RANS models [239,240], its high computational resource consumption hinders its widespread implementation.

6.2.2. Multiphase model

Synergistic wear is a complex phenomenon that involves three-phase flow of particles, liquid, and gas. The coupling of multiphase flows poses a significant challenge in calculation [241]. Commonly used multiphase flow models in CFD calculations include the Volume of Fluid (VOF), mixture multiphase, and Eulerian multiphase models. The VOF model [242] is used for flows that have a well-defined interface between phases. The mixture model [243] is a simplified Eulerian method where phases of the mixture can be fluid or particles, and are treated as an interspersed continuum. The velocities of particles and phases are assumed to be of the same size and direction. The relative velocity of the

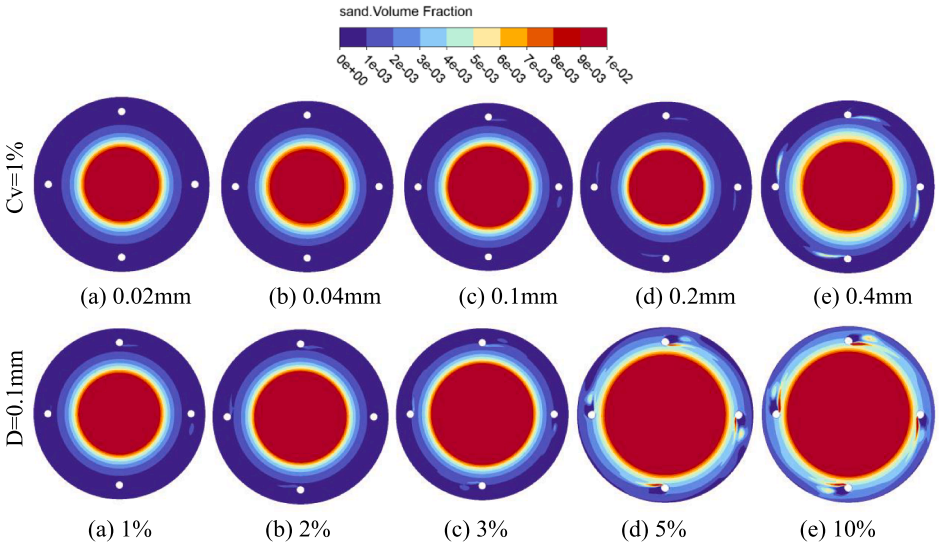

Fig. 29. Sand volume fraction on the surface of the rotating disk under different conditions [228].

Table 2
Numerical simulation of synergistic effect.

Research object	Cells	Particle parameters	Calculation model	Steady/ Transient	Code	Ref.
Single bubble	/	0.060–0.089 mm	VOF model	Transient	Fluent	[110]
Single guide vane and runner	/	0.005–0.1 mm; 1–5%	Homogeneous model; Singhal model	Steady	Fluent	[223]
Centrifugal pump	2,817,398	0.005–0.015 mm; 0.5–1.5%	Mixture model; Modified RNG $k-\varepsilon$; Schnerr-Sauer model	Steady	Fluent	[227]
Rotating disk	4,530,000	0.02–0.4 mm; 1–10%	Non-homogeneous model; ZGB model; Modified RNG $k-\varepsilon$ model	Steady	CFX	[228]
Rotary wear test rig	2,372,666	0.2 mm; 1.29 kg/m^3	Discrete phase model; Full cavitation model; Standard $k-\varepsilon$ model	Steady	Fluent	[208]
Butterfly valve	2,686,515	0.5 mm; 0.1%	Mixture model; DPM; Schnerr-Sauer model; Standard $k-\varepsilon$ model	Steady	Fluent	[224]
Slurry pot tester	/	106–150 μm; 3–10 wt%	Eulerian model; DPM; Realizable $k-\varepsilon$ model; User-defined synergy model	Transient	Fluent	[221]
Kaplan turbine	/	10–200 μm; 1000–10000 ppm	SST $k-\omega$ model; Discrete phase model	Steady	Fluent	[225]
Axial-flow pump	7,630,000	0.05–0.5 mm; 2–8%	Standard $k-\omega$ model; ZGB cavitation model	Steady	CFX	[226]
Francis turbine	5,592,825	3–5%	RNG $k-\varepsilon$ model; ZGB cavitation model; Eulerian model	Steady	CFX	[73]
Francis turbine	5,889,522	0.005–0.05 mm; 2–8%	SST $k-\omega$ model; zero equation model; ZGB cavitation model; Eulerian model	Steady	CFX	[230]
Venturi tube	510,100	0.023–0.063 mm; 25–75 kg/m^3	RNG $k-\varepsilon$ models; DPM	Transient	Fluent	[149]
Slurry pump	2,932,000	0.1–0.5 mm; 10–20%	Modified SAS-SST model; ZGB cavitation model; Eulerian model	Transient	CFX	[231]
Slurry pump	2,678,000	5–36 mm; 4–10%	Eulerian–Eulerian model	Steady	Fluent	[182]
Water tunnel	4,518,215	10–100 μm	Mixture model; Schnerr-Sauer model; Standard $k-\varepsilon/k-\omega$ model	Transient	Fluent	[197]

dispersed phase is determined by solving the momentum equation of the mixed fluid. The Eulerian model [244], also known as the two-fluid model, considers both media as continuous fluids. The two phases coexist at the same spatial point and penetrate each other, each obeying its mass, momentum, and energy equations. When the particle volume fraction is small (less than10%), the liquid and bubble are generally regarded as a fluid, and the particle is treated as a discrete phase. When the particle content is high, the particles can also be treated as part of the fluid. Hence, for multiphase flows containing discrete particles, the mathematical model describing the flow field is divided into Eulerian-Eulerian and Eulerian-Lagrangian methods.

The Eulerian-Lagrangian method has undergone three stages of development. The first stage involves a single-particle dynamics model that does not take into account the effect of the discrete relative continuous phase and the pulsation characteristics of the discrete phase. The second stage is characterized by the deterministic trajectory model, which considers the interaction between the discrete and continuous phases, but ignores the viscosity and turbulent diffusion characteristics of the discrete phase. In the third stage, the random trajectory model of the discrete phase is calculated, taking into account the effect of continuous phase turbulence on the discrete phase. This method is suitable for various sizes of low-concentration particle flows with complex motion processes. However, one of its drawbacks is that only discrete particles are treated as particles, making it difficult to give continuous spatial distribution information of parameters such as particle velocity and concentration. Moreover, it is challenging to fully consider the turbulent diffusion process of the mass and momentum of the discrete phase and its reaction to the continuous phase [245-247].

The method of Eulerian-Eulerian has undergone three developmental stages: (a) a model of a single fluid that treats the continuous and

discrete phases as one and disregards the difference in interphase velocity; (b) a small-slip model that takes into account a small amount of velocity slip between phases and disregards the effect of discrete phase relative to the continuous phase; and (c) a multi-fluid model that thoroughly considers interphase velocity slip, interphase coupling, and turbulent diffusion. In addition, the viscosity and diffusion coefficient of the discrete phase are introduced to reflect the turbulent transport issue of the discrete phase. Furthermore, the model considers the generation of turbulence, convection, diffusion, and extinction of the discrete phase under the continuous phase [246,248,249].

The numerical prediction of turbulence with particles poses several challenges. The Lagrangian method is more appropriate for single-phase coupling, while the two-fluid method is more suitable for two-phase coupling. Although DNS can provide an exemplary turbulence structure, particle dispersion, and two-way interaction between particles and turbulence, the high computing resource requirement needs to be taken into account [250]. When investigating three-phase flows involving particle-liquid–gas, the Eulerian-Eulerian method can comprehensively consider the interphase and turbulent diffusion forces resulting from sediment particles to the liquid. It is important to note that the liquid phase is typically considered incompressible and does not account for heat exchange [182].

6.2.3. Cavitation model

The most commonly used cavitation models include the Zwart-Gerber-Blemari model (ZGB) [251], the Kunz model [252], the Singhal model [253], and the Schnerr-Sauer model [254]. The ZGB model can be utilized in both mixture and Eulerian multiphase flow models simultaneously. It possesses good precision and convergence in calculations, making it the most widely used model. The Singhal model, also known as the complete cavitation model, considers the effect of uncondensed gas, which distinguishes it from other models. However, it cannot be used with the Eulerian multiphase model and is incompatible with the LES turbulence model. The model is better suited for simulating the reverse flow of cavitation and the vortex shedding of bubbles. To date, there is still no cavitation model capable of fully and accurately simulating various cavitation phenomena. To enhance the model's accuracy, one can adjust the empirical coefficient in the cavitation model and modify the turbulence model to account for the cavitation characteristics [231]. Additionally, when selecting the model, relevant factors such as the applicability and compatibility of the cavitation model to the multiphase flow model and the calculation convergence should also be considered [73].

6.3. Several complex problems in numerical simulation

6.3.1. Interphase forces of liquid–vapor-particle

The forces acting on particles in the cavitating fluid can be classified into four categories: (a) Forces that are not related to the relative motion between the fluid and the particles, including gravity, buoyancy, and pressure gradient force; (b) Forces, such as the Stokes force, virtual mass force, and Basset force, which depend on the relative motion between the fluid and the particles and oppose the direction of the relative motion velocity; (c) Forces related to the relative motion between the fluid and the particles, but with a direction perpendicular to the direction of relative motion velocity, including the Saffman force and Magnus force; (d) The force exerted on particles by the shock wave generated from bubble collapse.

The interaction between the phases involves both mass transfer and momentum transfer. Mass transfer refers to the exchange of mass between the liquid and gas phases caused by cavitation, while momentum transfer includes (a) the momentum transfer resulting from the interaction between the liquid-particle-vapor phases and (b) the momentum transfer resulting from mass transfer. The presence of particles in the fluid can increase both its inertia and viscosity, and particle motion may interact with the vortex flow of the continuous phase. The particle trailing flow may amplify fluid velocity pulsations [255], and the interphase drag force may also inhibit turbulence [256], which can affect the turbulent structure and ultimately alter flow stability. Therefore, it is necessary to consider and select interphase forces reasonably [257,258]. Li [259] and Dong [260] conducted a magnitude analysis of the interaction force between phases in terms of particle sizes. They suggested that the Basset force should not be neglected when the particle size is larger than 0.5 mm, and the virtual mass force should be considered when the particle size is greater than 2 mm. Furthermore, the Magnus force and Saffman force should be considered when the particle size exceeds 5 mm. Cao et al. [228,231] only took into account drag force, pressure gradient force, and turbulent diffusion force when considering the interphase force of the liquid–vapor-particle. Despite extensive discussion of interphase forces, the main issue is that there is no consensus on the choice of interphase force, and our understanding of particles' viscosity and turbulence effects remains incomplete [231].

6.3.2. Effect of particles on viscosity of mixed liquid

Previous experimental studies have shown that viscosity plays a critical role in the synergistic wear effect. The sediment diameter, sediment concentration, and temperature have a significant impact on wear by altering the viscosity of the mixed liquid [191]. In numerical simulations, the influence of changing mixed liquid viscosity on wear results is often neglected to simplify calculations, leading to deviations from field observations. When sediment particles are present in water flow, they introduce additional turbulence through disturbance, in addition to the turbulent viscosity of clear water. Particle Induced Eddy Viscosity has been researched by Sato and Sekoguchi [261], who modified the turbulent viscosity formula of liquid with particles. Turbulent viscosity of mixed liquid changes due to compressibility of the gas–liquid mixing zone during cavitation, and traditional turbulence models are often considered to overestimate actual turbulent viscosity in this case. Coutier-Delgosha [237] has proposed using a density correction function to rectify the density phase in the turbulent viscosity expression of RNG k-ε model, which has been recognized and applied by several scholars [262-264]. Zhang et al. [265] have incorporated this correction method into the SST k-ω model, resulting in improvements in numerical simulation work [228,231]. Tam and Zuber have also studied the treatment and correction formulas of multiphase flow viscosity. Despite the improved viscosity formulas' ability to enhance wear prediction accuracy, they are restricted by specific conditions and have limited applicability under the influence of high concentration and large particles [266-268]. Therefore, a universal formula that can predict the influence of particles and bubbles on the mixed liquid's viscosity needs further development and study.

6.3.3. Prediction of synergistic wear rate

The assessment and prediction of sediment erosion and cavitation are highly intricate tasks and depend on various factors, such as impact angle, particle velocity, flow conditions, geometric structure, and turbulent flow field [269]. Several models have been proposed to predict sediment erosion, including Finnie [270], Grant and Tabakoff [271], Oka [272,273], McLaury [274], and Zhang [275]. Predicting cavitation erosion is more challenging, as it requires the coupling of transient fatigue of the solid surface with the transient fluid. Presently, only a basic assessment of cavitation damage risk is possible [276-278], and some empirical or semi-empirical models for cavitation erosion have been proposed [279-281]. However, there is no numerical simulation model available to predict the combined wear rate. Trivedi and Dahlhaug [282] suggested that dynamic mesh and variable speed should be considered in studying transient CFD and FSI problems, which would further increase the complexity of numerical simulations.

In summary, the response to sediment-cavitation combined wear should address all potential problems [283]. In design, a reasonable choice of turbine type and working parameters [284], optimal hydraulic construction to deposit sediment in the reservoir [285], and using

materials with high resistance stability to sand and wear [286], along with protection technology [287], can effectively alleviate sediment impact and cavitation wear. Appropriate coatings can be applied to repair and maintain hydraulic machinery components, which is both economical and effective [288]. In experiments, the testing environment should resemble the natural flow situation, and the test time should be efficiently assessed [4]. In operation, maintenance, and repair, state-based monitoring technologies, such as fuzzy logic, analytic hierarchy process (AHP), particle swarm optimization (PSO), neural network, and self-organizing map (SOM) [289], can be used to classify and detect cavitation and particle wear. Machine learning methods can also be applied to monitor hydropower components [290], and supervisory control and data acquisition (SCADA), the Internet of Things, and cloud computing [291] can reduce the damage caused by sediment and cavitation, leading to optimal hydropower operation. In the future, further exploration of the combined mechanism requires a numerical simulation approach to reveal the changes in flow field and boundary parameters around bubbles, considering liquid compressibility [292], nanoscale cavitation [293,294], cavitation-shock wave interaction [295], particle-flow interaction [197], resonance effect [296], and fluid–structure interaction (FSI), which is essential to obtain accurate results. Thus, the use of FSI methods to solve sediment and cavitation erosion problems should receive more attention.

7. Conclusion and prospects

Although sediment erosion and cavitation damage have been the subject of study for a century, little is known about the underlying combined mechanism. The microscopic mechanism involves analyzing the motion behavior of particles and bubbles, which includes the trajectory, self-rotation, deformation, and acceleration of particles, as well as nucleation, non-spherical collapse, and bubble jetting of bubbles. As the bubble expands or collapses, particles may gain momentum, leading to acceleration and damage to the wall, primarily driven by micro-jets and pressure waves. The initial relative distance between the bubble and the particle is a critical determinant in triggering strong interaction. On a macroscopic level, the interaction between bubbles and particles is complex, resulting in two competing effects: synergistic inhibition and synergistic promotion. The particle and liquid properties can influence the generation and coalescence of free bubbles in a particle-bubble system, as well as the competition between viscous and inertial forces.

The interaction between bubbles and particles poses a challenging problem in transient fluid–solid coupling. To date, numerical studies of this phenomenon have primarily relied on potential flow theory and boundary element theory. While the widely acknowledged synergistic erosion model has not yet been established, there exist promising models that are worthy of further exploration. Currently, numerical simulations of cavitation in sediment-laden flow utilize coupling between cavitation and multiphase flow models. Nevertheless, the interaction between cavitation and particles is seldom accounted for, thereby hindering the precision of the obtained results. Achieving higher accuracy in numerical simulations requires careful consideration of the turbulence model, multiphase flow model, and cavitation model, as well as the influence of particles on liquid viscosity and the interaction between phases.

This paper explores the synergistic mechanism between bubbles and particles, its influencing factors, establishment of a combined model, and advanced numerical calculation methods. When developing a synergistic erosion model, it is important to fully consider the dual role of particles in synergistic erosion, as well as the impact of particles driven by micro jets or shock waves. In order to improve the reliability and accuracy of numerical calculations, future studies should focus on improving the influence of flow field and boundary parameters around bubbles, considering liquid compressibility, nanoscale cavitation, cavitation-shock wave interaction, particle-flow interaction, and resonance effects. Moreover, FSI should be utilized to predict wear location and erosion rate with greater accuracy. This study provides a comprehensive overview of the synergistic effect between cavitation and sediment, with the aim of enhancing our understanding of the combined wear mechanism of hydraulic machinery components in sediment-laden flow environments. This knowledge can be applied to the design, manufacturing, processing, maintenance, and operation of hydraulic machinery, and contribute to safe, stable, and optimized operation of power plants.

CRediT authorship contribution statement

Jie Sun: Writing – original draft. **Xinfeng Ge:** Writing – review & editing. **Ye Zhou:** Investigation. **Demin Liu:** Investigation. **Juan Liu:** Formal analysis. **Gaiye Li:** Formal analysis. **Yuan Zheng:** Supervision.

Declaration of Competing Interest

The authors declare that they have no known competing financial interests or personal relationships that could have appeared to influence the work reported in this paper.

Data availability

No data was used for the research described in the article.

Acknowledgement

The authors are thankful for the support of the National Natural Science Foundation of China (52279083).

References

[1] A. Kuriqi, A.N. Pinheiro, A. Sordo-Ward, M.D. Bejarano, L. Garrote, Ecological impacts of run-of-river hydropower plants—Current status and future prospects on the brink of energy transition, Renew. Sustain. Energy Rev. 142 (2021), 110833.
[2] D.E.H.J. Gernaat, P.W. Bogaart, D.P. van Vuuren, H. Biemans, R. Niessink, High-resolution assessment of global technical and economic hydropower potential, Nat. Energy 2 (2017) 821–828.
[3] Å. Killingtveit, 15 - Hydroelectric Power, in: T.M. Letcher (Ed.), Future Energy (Third Edition), Elsevier, 2020, pp. 315–330.
[4] A.A. Noon, M.-H. Kim, Sediment and Cavitation Erosion in Francis Turbines—Review of Latest Experimental and Numerical Techniques, Energies 14 (2021) 1516.
[5] Z. Mei, Y. Wu, Review of Research on Abrasion and Cavitation of Silt-Laden Flows Through Hydraulic Turbines in China, in: E. Cabrera, V. Espert, F. Martínez (Eds.), Hydraulic Machinery and Cavitation, Springer, Netherlands, Dordrecht, 1996, pp. 641–650.
[6] P. Kumar, R.P. Saini, Study of cavitation in hydro turbines—A review, Renew. Sustain. Energy Rev. 14 (2010) 374–383.
[7] B. Thapa, Sand Erosion in Hydraulic Machinery, Faculty of Engineering Ence & Technology. (2004).
[8] X. Song, R. Yao, Y. Shen, H. Bi, Y. Zhang, L. Du, Z. Wang, Numerical Prediction of Erosion Based on the Solid-Liquid Two-Phase Flow in a Double-Suction Centrifugal Pump, J. Marine Sci. Eng. 9 (2021) 836.
[9] A.K. Rai, A. Kumar, T. Staubli, X. Yexiang, Interpretation and application of the hydro-abrasive erosion model from IEC 62364 (2013) for Pelton turbines, Renew. Energy 160 (2020).
[10] K.R. Rakeshasharma, M.K. Padhy, A. Hota, S.K. Sarangi, A literature survey on silt erosion and cavitation in hydro turbine, in: 2016 International Conference on Signal Processing, Communication, Power and Embedded System (SCOPES), 2016: pp. 1771–1776.
[11] P.J. Dunstan, S.C. Li, Cavitation enhancement of silt erosion: Numerical studies, Wear 268 (2010) 946–954.
[12] Y. Zhang, Y. Zhang, Z. Qian, B. Ji, Y. Wu, A review of microscopic interactions between cavitation bubbles and particles in silt-laden flow, Renew. Sustain. Energy Rev. 56 (2016) 303–318.
[13] B. Gregorc, M. Hriberšek, A. Predin, The Analysis of the Impact of Particles on Cavitation Flow Development, J. Fluids Eng. 133 (2011), 111304.
[14] A.K. Rai, A. Kumar, T. Staubli, Effect of concentration and size of sediments on hydro-abrasive erosion of Pelton turbine, Renew. Energy 145 (2020) 893–902.
[15] M. Patel, B. Pardhi, M. Pal, Abrasive, Erosive and Corrosive Wear in Slurry Pumps -A Review 7 (2020) 2188–2195.
[16] D. Felix, I. Albayrak, A. Abgottspon, R.M. Boes, Hydro-abrasive erosion of hydraulic turbines caused by sediment - a century of research and development, IOP Conf. Ser.: Earth Environ. Sci. 49 (2016), 122001.

[17] S. Li, A.-M. Zhang, S. Wang, R. Han, Transient interaction between a particle and an attached bubble with an application to cavitation in silt-laden flow, Phys. Fluids 30 (2018), 082111.
[18] N. Ochiai, Y. Iga, M. Nohmi, T. Ikohagi, Study of Quantitative Numerical Prediction of Cavitation Erosion in Cavitating Flow, J. Fluids Eng. 135 (2013), 011302.
[19] N.S.M. Yusof, B. Babgi, Y. Alghamdi, M. Aksu, J. Madhavan, M. Ashokkumar, Physical and chemical effects of acoustic cavitation in selected ultrasonic cleaning applications, Ultrason. Sonochem. 29 (2016) 568–576.
[20] B.K. Sreedhar, S.K. Albert, A.B. Pandit, Cavitation damage: Theory and measurements – A review, Wear 372–373 (2017) 177–196.
[21] H. Kato, A. Konno, M. Maeda, H. Yamaguchi, Possibility of Quantitative Prediction of Cavitation Erosion Without Model Test, J. Fluids Eng. 118 (1996) 582–588.
[22] U. Dorji, R. Ghomashchi, Hydro turbine failure mechanisms: An overview, Eng. Fail. Anal. 44 (2014) 136–147.
[23] S. Hattori, E. Nakao, Cavitation erosion mechanisms and quantitative evaluation based on erosion particles, Wear 249 (2001) 839–845.
[24] M.C. Park, K.N. Kim, G.S. Shin, S.J. Kim, Effects of strain induced martensitic transformation on the cavitation erosion resistance and incubation time of Fe–Cr–Ni–C alloys, Wear 274–275 (2012) 28–33.
[25] W. Liu, Y.G. Zheng, C.S. Liu, Z.M. Yao, W. Ke, Cavitation erosion behavior of Cr–Mn–N stainless steels in comparison with 0Cr13Ni5Mo stainless steel, Wear 254 (2003) 713–722.
[26] Z. Li, J. Han, J. Lu, J. Zhou, J. Chen, Vibratory cavitation erosion behavior of AISI 304 stainless steel in water at elevated temperatures, Wear 321 (2014) 33–37.
[27] Y.G. Zheng, S.Z. Luo, W. Ke, Cavitation erosion–corrosion behaviour of CrMnB stainless overlay and 0Cr13Ni5Mo stainless steel in 0.5M NaCl and 0.5M HCL solutions, Tribol. Int. 41 (2008) 1181–1189.
[28] D. Ma, T.J. Harvey, Y.N. Zhuk, R.G. Wellman, R.J.K. Wood, Cavitation erosion performance of CVD W/WC coatings, Wear 452–453 (2020), 203276.
[29] D.G. Li, D.R. Chen, P. Liang, Enhancement of cavitation erosion resistance of 316 L stainless steel by adding molybdenum, Ultrason. Sonochem. 35 (2017) 375–381.
[30] H. Ganesh, S.A. Mäkiharju, S.L. Ceccio, Bubbly shock propagation as a mechanism for sheet-to-cloud transition of partial cavities, J. Fluid Mech. 802 (2016) 37–78.
[31] W.K. Soh, B. Willis, A flow visualization study on the movements of solid particles propelled by a collapsing cavitation bubble, Exp. Therm Fluid Sci. 27 (2003) 537–544.
[32] G. Bazanini, J.D. Bressan, M.A. Klemz, Cavitation Erosion Wear of Metallic Specimens Using the New Compact Rotating Disk Device, (2018).
[33] L. Yang, J. Wang, S. Chang, Effect of sediment-laden flow on cavitation pressure inside of hydraulic machineries in Wanjiazhai Hydropower Station, Water Resources and Hydropower, Engineering 36 (2005) 64–67.
[34] J. Chang, Decisive influence of the ionization strength of cosmic rays on the cavitation characteristics of pure water, Sci. China Ser. E-Technol. Sci. 52 (2009) 1804–1808.
[35] R. Shrestha, S.S. Pradhan, P. Gurung, A. Ghimire, S. Chitrakar, A review on erosion and erosion induced vibrations in Francis turbine, IOP Conf. Ser.: Earth Environ. Sci. (2022, 1037,), 012028.
[36] C. Peng, S. Tian, G. Li, M. Wei, Enhancement of cavitation intensity and erosion ability of submerged cavitation jet by adding micro-particles, Ocean Eng. 209 (2020), 107516.
[37] C.G. Duan, V.Y. Karelin, Abrasive erosion and corrosion of hydraulic machinery, 2003.
[38] W.A. Weyl, E.C. Marboe, Some Mechano-Chemical Properties of Water, US Office of Naval Report, 1948.
[39] H. Jin, F. Zheng, S. Li, C. Hang, The role of sand particles on the rapid destruction of the cavitation zone of hydraulic turbines, Wear 112 (1986) 199–205.
[40] R.J.K. Wood, S.P. Hutton, The synergistic effect of erosion and corrosion: trends in published results, Wear 140 (1990) 387–394.
[41] J. Sato, K. Usami, T. Okamura, Basic Study of Coupled Damage Caused by Silt Abrasion and Cavitation Erosion: Experiments with Submerged Water Jets, JSME Int. J. 34 (1991) 292–297.
[42] J. Madadnia, I. Owen, Accelerated surface erosion by cavitating particulate-laden flows, Wear 165 (1993) 113–116.
[43] K. Zhao, C. Gu, F. Shen, B. Lou, Study on mechanism of combined action of abrasion and cavitation erosion on some engineering steels, Wear 162–164 (1993) 811–819.
[44] J. Madadnia, I. Owen, Erosion in conical diffusers in particulate-laden cavitating flow, Int. J. Multiph. Flow 21 (1995) 1253–1257.
[45] S. Li, Cavitation enhancement of silt erosion-An envisaged micro model, Wear 260 (9–10) (2006) 1145–1150.
[46] V.K. Nanda, Parameters effecting abrasion and remedial measures. Silting Problems in Hydro Power Plants, CRC Press, 2000.
[47] K. Su, J. Wu, D. Xia, Classification of regimes determining ultrasonic cavitation erosion in solid particle suspensions, Ultrason. Sonochem. 68 (2020), 105214.
[48] W. Liu, Y.G. Zheng, Z.M. Yao, X.Q. Wu, W. Ke, Cavitation erosion of 20SiMn and 0Cr13Ni5Mo steels in distilled water with and without sand, IMR OpenIR. 37 (2001).
[49] C. Haosheng, W. Jiadao, C. Darong, Cavitation damages on solid surfaces in suspensions containing spherical and irregular microparticles, Wear 266 (2009) 345–348.
[50] H. Chen, S. Liu, J. Wang, D. Chen, Study on effect of microparticle's size on cavitation erosion in solid-liquid system, J. Appl. Phys. 101 (2007), 103510.
[51] J.R. Laguna-Camacho, R. Lewis, M. Vite-Torres, J.V. Méndez-Méndez, A study of cavitation erosion on engineering materials, Wear 301 (2013) 467–476.
[52] R.Y. Ting, Polymer effects on microjet impact and cavitation erosion, Nature 262 (1976) 572–573.
[53] H.X. Hu, Y.G. Zheng, The effect of sand particle concentrations on the vibratory cavitation erosion, Wear 384–385 (2017) 95–105.
[54] K.L. Sutherland, Physical Chemistry of Flotation, Kinetics of the Flotation Process, ACS Publications, XI, 2002.
[55] Y. Fu, X. Zhu, J. Wang, T. Gong, Numerical study of the synergistic effect of cavitation and micro-abrasive particles, Ultrason. Sonochem. 89 (2022), 106119.
[56] A. Rossetti, G. Pavesi, G. Ardizzon, A. Santolin, Numerical Analyses of Cavitating Flow in a Pelton Turbine, J. Fluids Eng. 136 (2014).
[57] B. Guo, Y. Xiao, A.K. Rai, J. Zhang, Q. Liang, Sediment-laden flow and erosion modeling in a Pelton turbine injector, Renew. Energy 162 (2020) 30–42.
[58] S. Chitrakar, H.P. Neopane, O.G. Dahlhaug, Study of the simultaneous effects of secondary flow and sediment erosion in Francis turbines, Renew. Energy 97 (2016) 881–891.
[59] R. Ramirez, E. Avila, L. Lopez, A. Bula, J. Duarte Forero, CFD characterization and optimization of the cavitation phenomenon in dredging centrifugal pumps, Alex. Eng. J. 59 (2020) 291–309.
[60] R. Shrestha, D. Bastakoti, H. Karn, I. Khadka, K.C. Khadananda, Transient Behavior at Hydropower Plants, 2012.
[61] B.S. Thapa, O.G. Dahlhaug, B. Thapa, Sediment erosion in hydro turbines and its effect on the flow around guide vanes of Francis turbine, Renew. Sustain. Energy Rev. 49 (2015) 1100–1113.
[62] L.A. Teran, R.D. Aponte, J. Muñoz-Cubillos, C.V. Roa, J.J. Coronado, J.A. Ladino, F.J. Larrahondo, S.A. Rodríguez, Analysis of economic impact from erosive wear by hard particles in a run-of-the-river hydroelectric plant, Energy 113 (2016) 1188–1201.
[63] A. Aslam Noon, M.-H. Kim, Erosion wear on Francis turbine components due to sediment flow, Wear (2017).
[64] M.K. Padhy, R.P. Saini, A review on silt erosion in hydro turbines, Renew. Sustain. Energy Rev. 12 (2008) 1974–1987.
[65] T.R. Bajracharya, B. Acharya, C.B. Joshi, R.P. Saini, O.G. Dahlhaug, Sand erosion of Pelton turbine nozzles and buckets: A case study of Chilime Hydropower Plant, Wear 264 (2008) 177–184.
[66] A. Kr, A. Rai, T.S. Kumar, Hydro-abrasive erosion in Pelton buckets: Classification and field study, Wear 392–393 (2017) 8–20.
[67] M.Z. Ud Din, G.A. Harmain, Assessment of erosive wear of Pelton turbine injector: Nozzle and spear combination – A study of Chenani hydro-power plant, Eng. Fail. Anal. 116 (2020), 104695.
[68] N.K. Mandal, Pelton runner erosion due to cavitation: a case study of storage hydropower plant, kulekhani first hydropower station, Thesis, Pulchowk Campus, 2021.
[69] T. Liao, H. Chen, T. Gao, W. Wang, B. Chen, T. Yang, F. Wang, Research on the size of sediment passing through the turbine effects on cavitation and cavitation erosion for the blade of three gorges hydropower plant, China Rural Water and Hydropower. (2012) 121-123+126.
[70] L.A. Teran, C.V. Roa, J. Muñoz-Cubillos, R.D. Aponte, J. Valdes, F. Larrahondo, S. A. Rodríguez, J.J. Coronado, Failure analysis of a run-of-the-river hydroelectric power plant, Eng. Fail. Anal. 68 (2016) 87–100.
[71] B. Cushman-Roisin, B. Jean-Marie, Introduction to Geophysical Fluid Dynamics: Physical and Numerical Aspects, Introduction to Geophysical Fluid Dynamics: Physical and Numerical Aspects, 2011.
[72] S. Chitrakar, H.P. Neopane, O.G. Dahlhaug, A Review on Sediment Erosion Challenges in Hydraulic Turbines, in: A. Amini (Ed.), Sedimentation Engineering, InTech, 2018.
[73] R. Zhang, Study on cavitation and wear of turbine runner in high sediment content water, Chongqing Jiaotong University, 2020. Thesis.
[74] B. Qian, L. Zhang, Y. Ma, X. Kong, Research on Abrasion Protection Technology of Hydroturbine Components in Gongzui Hydropower Station, IOP Conf. Ser.: Earth Environ. Sci. 453 (2020), 012063.
[75] P. Lin, D. Hu, Z. Lin, M. Liu, C. Tang, S. Wang, The mechanism of joint effects of axial-flow pump cavitation and sediment wear, Adv. Mech. Eng. 12 (2020).
[76] J.L. Lu, P.C. Guo, X.B. Zheng, Q. Zhao, X.Q. Luo, Numerical simulation of flow in centrifugal pump under cavitation and sediment condition, IOP Conf. Ser.: Earth Environ. Sci. 15 (2012), 032056.
[77] G. Silva, Wear Generation in Hydraulic Pumps, in: 1990: p. 901679.
[78] M. Mamajonov, D.R. Bazarov, B.R. Uralov, G.U. Djumabaeva, N. Rahmatov, The impact of hydro-wear parts of pumps for operational efficiency of the pumping station, J. Phys. Conf. Ser. 1425 (2019), 012123.
[79] K.C. Wilson, G.R. Addie, A. Sellgren, R. Clift, eds., Centrifugal Pumps, in: Slurry Transport Using Centrifugal Pumps, Springer US, Boston, MA, 2006: pp. 190–226.
[80] O. Glovatsky, R. Ergashev, B. Uralov, H. Isakov, Reliability assessment and measures for resource-saving in water lifting engine systems in Uzbekistan, Perpect. Innov. Econ. Bus. 4 (2010) 118–121.
[81] N. Qiu, L. Wang, S. Wu, D.S. Likhachev, Research on cavitation erosion and wear resistance performance of coatings, Eng. Fail. Anal. 55 (2015) 208–223.
[82] K. Su, J. Wu, D. Xia, Dual role of microparticles in synergistic cavitation–particle erosion: Modeling and experiments, Wear. v 470–471 (2021).
[83] R. Tarodiya, A. Levy, Surface erosion due to particle-surface interactions - A review, Powder Technol. 387 (2021) 527–559.
[84] S. Poulain, G. Guenoun, S. Gart, W. Crowe, S. Jung, Particle Motion Induced by Bubble Cavitation, Phys. Rev. Lett. 114 (2015), 214501.

[85] H. Murakawa, H. Kikura, M. Aritomi, Application of ultrasonic doppler method for bubbly flow measurement using two ultrasonic frequencies, Exp. Therm Fluid Sci. 29 (2005) 843–850.
[86] H. Murakawa, H. Kikura, M. Aritomi, Application of ultrasonic multi-wave method for two-phase bubbly and slug flows, Flow Meas. Instrum. 19 (2008) 205–213.
[87] X. Zhan, Y. Yang, J. Liang, T. Shi, X. Li, Gas Bubble Effects and Elimination in Ultrasonic Measurement of Particle Concentrations in Solid-Liquid Mixing Processes, IEEE Trans. Instrum. Meas. 66 (2017) 1711–1718.
[88] R. Altay, A.K. Sadaghiani, M.I. Sevgen, A. Şişman, A. Koşar, Numerical and Experimental Studies on the Effect of Surface Roughness and Ultrasonic Frequency on Bubble Dynamics in Acoustic Cavitation, Energies 13 (2020) 1126.
[89] A. Shukla, A. Prakash, Ultrasonic technique to determine particle size and concentration in slurry systems, Chem. Eng. Sci. 61 (2006) 2468–2475.
[90] S. L, Cavitation Enhancement in silt erosion: obstacles & way forward, in: Proceedings of the Fifth International Symposium on Cavitation, Osaka, Japan, 1–4 November 2003, n.d.
[91] T.-H. Kim, H.-Y. Kim, Disruptive bubble behaviour leading to microstructure damage in an ultrasonic field, J. Fluid Mech. 750 (2014) 355–371.
[92] S. Mitra, M. Mainul Hoque, G. Evans, A.V. Nguyen, Direct visualisation of bubble-particle interactions in presence of cavitation bubbles in an ultrasonic flotation cell, Miner. Eng. 174 (2021), 107258.
[93] X. Wang, G. Wu, X. Zheng, X. Du, Y. Zhang, Y. Zhang, Theoretical investigation and experimental support for the cavitation bubble dynamics near a spherical particle based on Weiss theorem and Kelvin impulse, Ultrason. Sonochem. 89 (2022), 106130.
[94] L. Lv, Y. Zhang, Y. Zhang, Y. Zhang, Experimental investigations of the particle motions induced by a laser-generated cavitation bubble, Ultrason. Sonochem. 56 (2019) 63–76.
[95] W. Xu, Y. Zhang, J. Luo, Q. Arong, Y.Z. Zhang, The impact of particles on the collapse characteristics of cavitation bubbles, Ocean Eng. 131 (2017) 15–24.
[96] S.R. Gonzalez-Avila, X. Huang, P.A. Quinto-Su, T. Wu, C.-D. Ohl, Motion of Micrometer Sized Spherical Particles Exposed to a Transient Radial Flow: Attraction, Repulsion, and Rotation, Phys. Rev. Lett. 107 (2011), 074503.
[97] S. Wu, B. Li, Z. Zuo, S. Liu, Dynamics of a single free-settling spherical particle driven by a laser-induced bubble near a rigid boundary, Phys. Rev. Fluids 6 (2021), 093602.
[98] L. Zhang, V. Belova, H. Wang, W. Dong, H. Möhwald, Controlled Cavitation at Nano/Microparticle Surfaces, Chem. Mater. 26 (2014) 2244–2248.
[99] Y. Zhang, F. Chen, Y. Zhang, Y. Zhang, X. Du, Experimental investigations of interactions between a laser-induced cavitation bubble and a spherical particle, Exp. Therm Fluid Sci. 98 (2018) 645–661.
[100] Y. Tomita, P.B. Robinson, R.P. Tong, J.R. Blake, Growth and collapse of cavitation bubbles near a curved rigid boundary, J. Fluid Mech. 466 (2002) 259–283.
[101] J. Chang, Cavitation and cavitation erosion of pump and turbine with silt-laden water as working medium, Paiguan Jixie Gongcheng Xuebao/Journal of Drainage and Irrigation Machinery Engineering. 28 (2) (2010) 93–97.
[102] M. Arora, C.-D. Ohl, K.A. Mørch, Cavitation Inception on Microparticles: A Self-Propelled Particle Accelerator, Phys. Rev. Lett. 92 (2004), 174501.
[103] B.M. Borkent, M. Arora, C.-D. Ohl, N. De Jong, M. Versluis, D. Lohse, K.A. Mørch, E. Klaseboer, B.C. Khoo, The acceleration of solid particles subjected to cavitation nucleation, J. Fluid Mech. 610 (2008) 157–182.
[104] A. Abouel-Kasem, S.M. Ahmed, Cavitation Erosion Mechanism Based on Analysis of Erosion Particles, J. Tribol. 130 (2008), 031601.
[105] H.B. Marschall, K.A. Mørch, A.P. Keller, M. Kjeldsen, Cavitation inception by almost spherical solid particles in water, Phys. Fluids 15 (2003) 545–553.
[106] B.M. Borkent, M. Arora, C.-D. Ohl, Reproducible cavitation activity in water-particle suspensions, J. Acoust. Soc. Am. 121 (2007) 1406–1412.
[107] Z.A. Zhou, Z. Xu, J.A. Finch, Effect of Surface Properties of Fine Particles on Dynamic Bubble Formation in Gas-Supersaturated Systems, Ind. Eng. Chem. Res. 37 (1998) 1998–2004.
[108] V. Belova, D.A. Gorin, D.G. Shchukin, H. Möhwald, Controlled Effect of Ultrasonic Cavitation on Hydrophobic/Hydrophilic Surfaces, ACS Appl. Mater. Interfaces 3 (2011) 417–425.
[109] C. Gungoren, O. Ozdemir, X. Wang, S.G. Ozkan, J.D. Miller, Effect of ultrasound on bubble-particle interaction in quartz-amine flotation system, Ultrason. Sonochem. 52 (2019) 446–454.
[110] L.A. Teran, S.A. Rodríguez, S. Laín, S. Jung, Interaction of particles with a cavitation bubble near a solid wall, Phys. Fluids 30 (2018), 123304.
[112] S.-W. Ohl, D.W. Wu, E. Klaseboer, B.C. Khoo, Spark bubble interaction with a suspended particle, J. Phys. Conf. Ser. 656 (2015), 012033.
[113] R.M. Wagterveld, L. Boels, M.J. Mayer, G.J. Witkamp, Visualization of acoustic cavitation effects on suspended calcite crystals, Ultrason. Sonochem. 18 (2011) 216–225.
[114] S. Wu, Z. Zuo, H.A. Stone, S. Liu, Motion of a Free-Settling Spherical Particle Driven by a Laser-Induced Bubble, Phys. Rev. Lett. 119 (2017), 084501.
[115] M. Xu, C. Ji, J. Zou, X. Ruan, X. Fu, Particle removal by a single cavitation bubble, Sci. China Phys. Mech. Astron. 57 (2014) 668–673.
[116] D. Pavard, E. Klaseboer, S.-W. Ohl, B.C. Khoo, Removal of particles from holes in submerged plates with oscillating bubbles, Phys. Fluids 21 (2009), 083304.
[117] K.L. Tan, S.H. Yeo, Velocity estimation of micro-particles driven by cavitation bubble collapses through controlled erosion experiments, Int. J. Multiph. Flow 127 (2020), 103271.
[118] S.-Y. Chen, W.-L. Xu, J. Luo, J.-B. Li, Y.-W. Zhai, Experimental study on the mesoscale causes of the effect of sediment size and concentration on material cavitation erosion in sandy water, Wear 488–489 (2022), 204114.
[119] T. Koita, K. Hayashi, M. Sun, Experimental Study of Underwater Shock Wave and Cavitation Generated by Underwater Electric Discharge in a Narrow Container, in: R. Bonazza, D. Ranjan (Eds.), 29th International Symposium on Shock Waves 2, Springer International Publishing, Cham, 2015, pp. 1505–1510.
[120] E.A. Brujan, T. Ikeda, K. Yoshinaka, Y. Matsumoto, The final stage of the collapse of a cloud of bubbles close to a rigid boundary, Ultrason. Sonochem. 18 (2011) 59–64.
[121] K.A. Kusters, S.E. Pratsinis, S.G. Thoma, D.M. Smith, Ultrasonic fragmentation of agglomerate powders, Chem. Eng. Sci. 48 (1993) 4119–4127.
[122] F. Wang, I. Tzanakis, D. Eskin, J. Mi, T. Connolley, In situ observation of ultrasonic cavitation-induced fragmentation of the primary crystals formed in Al alloys, Ultrason. Sonochem. 39 (2017) 66–76.
[123] F. Wang, D. Eskin, J. Mi, C. Wang, B. Koe, A. King, C. Reinhard, T. Connolley, A synchrotron X-radiography study of the fragmentation and refinement of primary intermetallic particles in an Al-35 Cu alloy induced by ultrasonic melt processing, Acta Mater. 141 (2017) 142–153.
[124] S. Sumitomo, H. Koizumi, M.A. Uddin, Y. Kato, Comparison of dispersion behavior of agglomerated particles in liquid between ultrasonic irradiation and mechanical stirring, Ultrason. Sonochem. 40 (2018) 822–831.
[125] J. Xiang, Research on the breakage of fine particles under cavitation impact in liquid phase, Zhejiang University of Technology, 2018. Thesis.
[126] L. Zhu, Research on the crushing effect of fine particles under effective impact of cavitating jet coupled with medium collision, Zhejiang University of Technology, 2020. Thesis.
[127] S. Huang, The effect of ultrasonic cavitation on fine particle breakage around rigid wall under rotating flow field, Zhejiang University of Technology, 2019. Thesis.
[128] O. Supponen, D. Obreschkow, P. Kobel, N. Dorsaz, M. Farhat, Detailed experiments on weakly deformed cavitation bubbles, Exp. Fluids 60 (2019) 33.
[129] O. Supponen, D. Obreschkow, P. Kobel, M. Tinguely, N. Dorsaz, M. Farhat, Shock waves from nonspherical cavitation bubbles, Phys. Rev. Fluids 2 (2017), 093601.
[130] L. Xian, Research on the effects of silt mean diameters and silt concentrations on transient cavitation of hydrofoil and centrifugal pump, Lanzhou University of Technology, 2018. Thesis.
[131] O. Supponen, D. Obreschkow, M. Tinguely, P. Kobel, N. Dorsaz, M. Farhat, Scaling laws for jets of single cavitation bubbles, J. Fluid Mech. 802 (2016) 263–293.
[132] Y. Shi, Study on the Characteristics of Laser-induced Bubble and the Mechanism of Cavitation Erosion in Sand-laden Condition, Jiangsu University, 2019. Thesis.
[133] Y. Zhang, X. Xie, Y. Zhang, Y. Zhang, High-speed experimental photography of collapsing cavitation bubble between a spherical particle and a rigid wall, J. Hydrodyn. 30 (2018) 1012–1021.
[134] M. Yuan, C. Li, J. Ge, Q. Xu, Z. Li, Study on the Motion Characteristics of Solid Particles in Fine Flow Channels by Ultrasonic Cavitation, Micromachines 13 (2022) 1196.
[135] T. Tuziuti, K. Yasui, M. Sivakumar, Y. Iida, N. Miyoshi, Correlation between Acoustic Cavitation Noise and Yield Enhancement of Sonochemical Reaction by Particle Addition, Chem. A Eur. J. 109 (2005) 4869–4872.
[136] Z.A. Zhou, Z. Xu, J.A. Finch, On the role of cavitation in particle collection during flotation - a critical review, Miner. Eng. 7 (1994) 1073–1084.
[137] T.-H. Phan, V.-T. Nguyen, T.-N. Duy, D.-H. Kim, W.-G. Park, Influence of phase-change on the collapse and rebound stages of a single spark-generated cavitation bubble, Int. J. Heat Mass Transf. 184 (2022), 122270.
[138] G. Sinibaldi, A. Occhicone, F. Alves Pereira, D. Caprini, L. Marino, F. Michelotti, C.M. Casciola, Laser induced cavitation: Plasma generation and breakdown shockwave, Phys. Fluids 31 (2019), 103302.
[139] J.M. Rosselló, W. Lauterborn, M. Koch, T. Wilken, T. Kurz, R. Mettin, Acoustically induced bubble jets, Phys. Fluids 30 (2018), 122004.
[140] X. Zhang, T. Inada, A. Yabe, S. Lu, Y. Kozawa, Active control of phase change from supercooled water to ice by ultrasonic vibration 2. Generation of ice slurries and effect of bubble nuclei, Int. J. Heat Mass Transf. 44 (2001) 4533–4539.
[141] Z. Xiangqing, Z. Yuning, Experimental investigation of the influences of the spherical particle on the jet formation of the cavitation bubble near the solid boundary, Mech. Eng. 43 (2021) 506.
[142] T. Prozorov, R. Prozorov, K.S. Suslick, High Velocity Interparticle Collisions Driven by Ultrasound, J. Am. Chem. Soc. 126 (2004) 13890–13891.
[143] J. Ma, C.-T. Hsiao, G.L. Chahine, Numerical study of acoustically driven bubble cloud dynamics near a rigid wall, Ultrason. Sonochem. 40 (2018) 944–954.
[144] Y. Zhang, X. Xie, Y. Zhang, Y. Zhang, X. Du, Experimental study of influences of a particle on the collapsing dynamics of a laser-induced cavitation bubble near a solid wall, Exp. Therm Fluid Sci. 105 (2019) 289–306.
[145] R.L. Howard, A. Ball, The solid particle and cavitation erosion of titanium aluminide intermetallic alloys, Wear 186–187 (1995) 123–128.
[146] B. Rajkarnikar, H.P. Neopane, B.S. Thapa, Development of rotating disc apparatus for test of sediment-induced erosion in Francis runner blades, Wear 306 (2013) 119–125.
[147] L. Lu, J. Liu, J.G. Zhang, L. Zhu, H.Q. Xu, X.C. Meng, J.C. Yu, S.P. Ma, K. Wang, An experiment system for testing synergetic erosion caused by sand abrasion and cavitation, IOP Conf. Ser.: Earth Environ. Sci. 22 (2014), 052017.
[148] J. Zhang, M.O.W. Richardson, G.D. Wilcox, J. Min, X. Wang, Assessment of resistance of non-metallic coatings to silt abrasion and cavitation erosion in a rotating disk test rig, Wear 194 (1996) 149–155.
[149] K. Luo, Mechanism study of cavitation erosion and sand erosion of sediment slurry in venturi, Jiangsu University, 2020. Thesis.
[150] T. Okada, Y. Iwai, S. Hattori, N. Tanimura, Relation between impact load and the damage produced by cavitation bubble collapse, Wear 184 (1995) 231–239.

[151] V. Matikainen, H. Koivuluoto, P. Vuoristo, A study of Cr3C2-based HVOF- and HVAF-sprayed coatings: Abrasion, dry particle erosion and cavitation erosion resistance, Wear 446–447 (2020), 203188.
[152] T. Zhang, C. Chen, D. Luml, D. Li, Mechanism of silt abrasion enhanced by cavitation in silt laden water flow, Paiguan Jixie Gongcheng Xuebao/J. Drainage Irrigation Machinery Engineering 29 (4) (2011) 297–302.
[153] Z. Tao, C. Chen, L. Dan, D. Lv, Experimental study of mechanism of silt abrasion influenced by cavitation in hydraulic machinery, ASME-JSME-KSME, Joint Fluids Eng. Conf. 1 (Parts A,B,C,D) (2011) 195–201.
[154] B. Gregorc, A. Predin, D. Fabijan, R. Klasinc, Experimental Analysis of the Impact of Particles on the Cavitating Flow, SV-JME. 58 (2012) 238–244.
[155] S. Lv, Simulation of hydrofoil cavitation caused by angle of attack and sediment, Xi'an University of Technology, Thesis, 2020.
[156] H.J. Amarendra, G.P. Chaudhari, S.K. Nath, Synergy of cavitation and slurry erosion in the slurry pot tester, Wear 290 (2012) 25–31.
[157] B. Thapa, P. Chaudhary, O.G. Dahlhaug, P. Upadhyay, Study of combined effect of sand erosion and cavitation in hydraulic turbines, in: International Conference on Small Hydropower-Hydro Sri Lanka, Citeseer, 2007: p. 24.
[158] D.G. Li, Y. Long, P. Liang, D.R. Chen, Effect of micro-particles on cavitation erosion of Ti6Al4V alloy in sulfuric acid solution, Ultrason. Sonochem. 36 (2017) 270–276.
[159] J. Stella, R. Alcivar, Influence of addition of microsized alumina particles on material damage induced by vibratory cavitation erosion, Wear 436–437 (2019), 203027.
[160] S. Huang, A. Ihara, H. Watanabe, H. Hashimoto, Effects of Solid Particle Properties on Cavitation Erosion in Solid-Water Mixtures, J. Fluids Eng. 118 (1996) 749–755.
[161] J. Wang, H. Chen, L. Qin, Y. Li, D. Chen, Key roles of micro-particles in water on occurrence of cavitation-erosion of hydro-machinery, Sci. Bull. 53 (2008) 1603–1607.
[162] H. Chen, D. Sun, Y. Wu, M. Chen, P. Zhang, Effect of Solid Particles on Cavitation and Lubrication Characteristics of Upstream Pumping Mechanical Seal Liquid Membrane, Int. J. Fluid Mach. Systems. 10 (2017) 412–420.
[163] W. Gou, H. Zhang, H. Li, F. Liu, J. Lian, Effects of silica sand on synergistic erosion caused by cavitation, abrasion, and corrosion, Wear 412–413 (2018) 120–126.
[164] R. Singh, S.K. Tiwari, S.K. Mishra, Cavitation Erosion in Hydraulic Turbine Components and Mitigation by Coatings: Current Status and Future Needs, J. Mater. Eng. Perform. 21 (2012) 1539–1551.
[165] P.P. Gohil, R.P. Saini, Coalesced effect of cavitation and silt erosion in hydro turbines-A review, Renew. Sust. Energ. Rev. 33 (2014) 280–289.
[166] C. Guo, J. Liu, X. Li, S. Yang, Effect of cavitation bubble on the dispersion of magnetorheological polishing fluid under ultrasonic preparation, Ultrason. Sonochem. 79 (2021), 105782.
[167] Y. Li, Study on mechanism of surface topograhpy effects on generation of cavitation erosion, Tsinghua University, 2009. Thesis.
[168] H. Chen, Effect of microparticles on ultrasonic cavitation damage, North China University of Technology, 2021. Thesis.
[169] P. Zhang, Research on laser-induced cavitation characteristics and cavitation corrosion mechanism of 6061 aluminum alloy in sandy water environments, Jiangsu University, 2021. Thesis.
[170] J. Wu, W. Gou, Critical size effect of sand particles on cavitation damage, J. Hydrodyn. 25 (2013) 165–166.
[171] J. Lian, W. Gou, H. Li, H. Zhang, Effect of sediment size on damage caused by cavitation erosion and abrasive wear in sediment-water mixture, Wear 398–399 (2018) 201–208.
[172] W. Gou, J. Wu, H. Zhang, J. Lian, Simulation Modeling of the Combined Damage Caused by Cavitation and Abrasion in Sediment-Laden Liquids, J. Fluids Eng. 140 (2018).
[173] X. Liu, J. He, J. Lu, X. Ni, Effect of Liquid Viscosity on a Liquid Jet Produced by the Collapse of a Laser-Induced Bubble near a Rigid Boundary, Jpn. J. Appl. Phys. 48 (2009), 016504.
[174] Y. Wang, J. Wu, F. Ma, Cavitation–silt erosion in sand suspensions, J. Mech. Sci. Technol. 32 (2018) 5697–5702.
[175] S. Bahadur, R. Badruddin, Erodent particle characterization and the effect of particle size and shape on erosion, Wear 138 (1990) 189–208.
[176] M. Liebhard, A. Levy, The effect of erodent particle characteristics on the erosion of metals, Wear 151 (1991) 381–390.
[177] A.V. Levy, P. Chik, The effects of erodent composition and shape on the erosion of steel, Wear 89 (1983) 151–162.
[178] G.R. Desale, B.K. Gandhi, S.C. Jain, Effect of erodent properties on erosion wear of ductile type materials, Wear 261 (2006) 914–921.
[179] E.N. Harvey, D. Wm, A.H.W. McElroy, On Cavity Formation in Water, J. Appl. Phys. 18 (1947) 162–172.
[180] L. Wang, R. Sha, J. Chang, Effect of sand concentration in water on cavitation pressure in Qingtongxia and Bapanxia hydropower stations, J. Hydroelectric Eng. (2008) 44–47.
[181] S. Hong, Y. Wu, Q. Wang, G. Ying, G. Li, W. Gao, B. Wang, W. Guo, Microstructure and cavitation-silt erosion behavior of high-velocity oxygen-fuel (HVOF) sprayed Cr3C2-NiCr coating, Surface Coatings Technol. 225 (2013) 85–91.
[182] Cavitation performance of multistage slurry pump in deep-sea mining, AIP Advances. 9 (2019) 105024.
[183] D. Stoian, N. Eshtiaghi, J. Wu, R. Parthasarathy, Intensification of sonochemical reactions in solid-liquid systems under fully suspended condition, Chem. Eng. Process. - Process Intesif. 123 (2018) 34–44.
[184] R. Romero, L.A. Teran, J.J. Coronado, J.A. Ladino, S.A. Rodríguez, Synergy between cavitation and solid particle erosion in an ultrasonic tribometer, Wear. 428–429 (2019) 395–403.
[185] K. Su, J. Wu, D. Xia, Z. Ding, Cavitation damage in particle-laden liquids with considering particle concentration and size, in: Sapporo, Japan, 2020: pp. 1–6.
[186] D. Yan, J. Wang, F. Liu, Inhibition of the ultrasonic microjet-pits on the carbon steel in the particles-water mixtures, AIP Adv. 5 (2015), 077159.
[187] J. Wu, K. Su, Y. Wang, W. Gou, Effect of air bubble size on cavitation erosion reduction, Sci. China Technol. Sci. 60 (2017) 523–528.
[188] V. Ashworth, R.P.M. Procter, Cavitation damage in dilute polymer solutions, Nature 258 (1975) 64–66.
[189] N. Phan-Thien, D.C. Pham, Differential multiphase models for polydispersed suspensions and particulate solids, J. Nonnewton. Fluid Mech. 72 (1997) 305–318.
[190] J. Happel, Viscosity of Suspensions of Uniform Spheres, J. Appl. Phys. 28 (1957) 1288–1292.
[191] J. Wu, Y. Wang, F. Ma, W. Gou, Cavitation erosion in bloods, Journal of Hydrodynamics, Ser. B. 29 (2017) 724–727.
[192] A. Einstein, Eine neue bestimmung der moleküldimensionen, ETH Zurich, 1905.
[193] D.G. Thomas, Transport characteristics of suspension: VIII. A note on the viscosity of Newtonian suspensions of uniform spherical particles, J. Colloid Sci. 20 (1965) 267–277.
[194] J. Huang, Effect of liquid viscosity on bubble living process, J. Beijing Inst. Civil Eng. Architecture 2 (1994) 124–131.
[195] J. Huang, Effect of sediment concentration on bubble expansion and collapse process in fluids with different surface tension, J. Hydraul. Eng. (1998).
[196] J.M. Truby, S.P. Mueller, E.W. Llewellin, H.M. Mader, The rheology of three-phase suspensions at low bubble capillary number, Proceedings of the Royal Society A: Mathematical, Physical and Engineering Sciences. 471 (2015) 20140557.
[197] H. Shi, Q. Liu, P. Nikrityuk, Modeling of cavitating flows past a micro-sized particle, Int. J. Multiph. Flow 128 (2020), 103276.
[198] C.M. Phan, A.V. Nguyen, J.D. Miller, G.M. Evans, G.J. Jameson, Investigations of bubble–particle interactions, Int. J. Miner. Process. 72 (2003) 239–254.
[199] D. Wan, X. Yi, L.-P. Wang, X. Sun, S. Chen, G. Wang, Study of collisions between particles and unloaded bubbles with point-particle model embedded in the direct numerical simulation of turbulent flows, Miner. Eng. 146 (2020), 106137.
[200] M. Firouzi, A.V. Nguyen, S.H. Hashemabadi, The effect of microhydrodynamics on bubble–particle collision interaction, Miner. Eng. 24 (2011) 973–986.
[201] K.L. Sutherland, Physical Chemistry of Flotation. XI. Kinetics of the Flotation Process, J. Phys. Chem. 52 (1948) 394–425.
[202] Z.A. Zhou, Z. Xu, J.A. Finch, J.H. Masliyah, R.S. Chow, On the role of cavitation in particle collection in flotation – A critical review, II, Minerals Engineering. 22 (2009) 419–433.
[203] B.M. Borkent, S. Gekle, A. Prosperetti, D. Lohse, Nucleation threshold and deactivation mechanisms of nanoscopic cavitation nuclei, Phys. Fluids 21 (2009), 102003.
[204] S. Gopalan, J. Katz, Flow structure and modeling issues in the closure region of attached cavitation, Phys. Fluids 12 (2000) 895–911.
[205] Y. Long, X. Long, B. Ji, H. Huang, Numerical simulations of cavitating turbulent flow around a marine propeller behind the hull with analyses of the vorticity distribution and particle tracks, Ocean Eng. 189 (2019), 106310.
[206] Controlled hydrodynamic cavitation erosion with abrasive particles for internal surface modification of additive manufactured components, Wear. 414–415 (2018) 89–100.
[207] H. Nanjo, A. Shima, T. Tsujino, Formation of damage pits by cavitation in a polymer solution, Nature 320 (1986) 516–517.
[208] Y. Pang, L. Liang, Y. Tang, Z. Zhu, Numerical analysis and experimental investigation of combined erosion of cavitation and sandy water erosion, Proc. Inst. Mech. Eng., Part J: J. Eng. Tribol. 230 (2016) 31–39.
[209] G.F. Truscott, A literature survey on abrasive wear in hydraulic machinery, Wear 20 (1972) 29–50.
[210] T. Nozaki, T. Takayanagi, Estimation of repair cycle of turbine due to abrasion caused by suspended sand and determination of capacity and cross section of desilting basin, Dengen Kaihatsu K.K., Chosa Shiryo; (Japan). 81 (1987).
[211] M.S. Bingley, D.J. O'Flynn, Examination and comparison of various erosive wear models, Wear 258 (2005) 511–525.
[212] G. Prashar, H. Vasudev, L. Thakur, Performance of different coating materials against slurry erosion failure in hydrodynamic turbines: A review, Eng. Fail. Anal. 115 (2020), 104622.
[213] P.J. Harris, A numerical method for predicting the motion of a bubble close to a moving rigid structure, Commun. Numer. Methods Eng. 9 (1993) 81–86.
[214] J.H. Duncan, S. Zhang, On the interaction of a collapsing cavity and a compliant wall, J. Fluid Mech. 226 (1991) 401–423.
[215] S. Li, R. Han, A.M. Zhang, Nonlinear interaction between a gas bubble and a suspended sphere, J. Fluids Struct. 65 (2016) 333–354.
[216] S. Li, A.M. Zhang, R. Han, Y.Q. Liu, Experimental and numerical study on bubble-sphere interaction near a rigid wall, Phys. Fluids 29 (2017), 092102.
[217] G.L. Chahine, A. Kapahi, J.-K. Choi, C.-T. Hsiao, Modeling of surface cleaning by cavitation bubble dynamics and collapse, Ultrason. Sonochem. 29 (2016) 528–549.
[218] G.L. Chahine, C.-T. Hsiao, Modelling cavitation erosion using fluid–material interaction simulations, Interface Focus. 5 (2015) 20150016.
[219] S. Li Bubble–boundary interaction Cavitation of Hydraulic Machinery, ICP 2000 London.

[220] L. Lv, Experimental Investigations of the Mechanisms of the Interaction between a Cavitation Bubble and Spherical Particles, China University of Petroleum, 2019. Thesis.
[221] L.A. Teran, S. Laín, S.A. Rodríguez, Synergy effect modelling of cavitation and hard particle erosion: Implementation and validation, Wear 478–479 (2021), 203901.
[222] J. Zevnik, M. Dular, Cavitation bubble interaction with a rigid spherical particle on a microscale, Ultrason. Sonochem. 69 (2020), 105252.
[223] L. Weili, L. Jinling, L. Xingqi, L. Yuan, Research on the cavitation characteristic of Kaplan turbine under sediment flow condition, in: IOP Conference Series: Earth and Environmental Science, IOP Publishing, 2010, p. 012022.
[224] B. Liu, J. Zhao, J. Qian, Numerical analysis of cavitation erosion and particle erosion in butterfly valve, Eng. Fail. Anal. 80 (2017) 312–324.
[225] D. Kumar, P.P. Bhingole, CFD Based Analysis of Combined Effect of Cavitation and Silt Erosion on Kaplan Turbine, Mater. Today:. Proc. 2 (2015) 2314–2322.
[226] P. Lin, D. Hu, J.-M. Lu, S. Wang, CFD numerical simulation of sand-contained cavitation characteristics of axial-flow pump, Adv. Mech. Eng. 13 (2021).
[227] W. Zhao, X. Han, R. Li, Y. Zheng, X. Pan, Effects of silt diameter and silt concentration on cavitation flow in centrifugal pump, Nongye Gongcheng Xuebao/Transactions of the Chinese Society of, Agri. Eng. 33 (4) (2017) 117–124.
[228] J. Sun, X. Ge, D. Chu, L. Zhang, H. Meng, Y. Zheng, Effects of sediment diameter and concentration on cavitation characteristics and mechanism, Tribol. Int. 171 (2022), 107543.
[229] W. Zhao, X. Han, R. Li, Y. Zheng, Y. Wang, Effects of size and concentration of silt particles on flow and performance of a centrifugal pump under cavitating conditions, Mod. Phys. Lett. B (2017).
[230] J. Wang, Cavitation characteristics of francis turbine under sediment-laden flow, Zhejiang University, 2016. Thesis.
[231] L. Cao, Research on unsteady characteristics of silt-laden cavitating flow in a centrifugal dredging pump, Tsinghua University, 2017. Thesis.
[232] A. Inc, ANSYS Fluent Theory Guide, (2013).
[233] G.H. Yeoh, J. Tu, Computational Techniques for Multiphase Flows, Computational Techniques for Multiphase Flows. (2010).
[234] Z. Han, R.D. Reitz, Turbulence Modeling of Internal Combustion Engines Using RNG κ-ε Models, Combust. Sci. Technol. 106 (1995) 267–295.
[235] D.-S. Zhang, G.-G. Zhang, H.-Y. Wang, W.-D. Shi, Numerical investigation of time-dependent cloud cavitating flow around a hydrofoil, Therm. Sci. 20 (2016) 913–920.
[236] O. Coutier-Delgosha, R. Fortes-Patella, J.L. Reboud, Simulation of unsteady cavitation with a two-equation turbulence model including compressibility effects, JoT. 3 (2002) N58.
[237] O. Coutier-Delgosha, R.F. Patella, J.L. Reboud, Evaluation of the turbulence model influence on the numerical simulations of unsteady cavitation, J. Fluids Eng. (2008).
[238] B. Ji, X. Luo, Y. Wu, X. Peng, Y. Duan, Numerical analysis of unsteady cavitating turbulent flow and shedding horse-shoe vortex structure around a twisted hydrofoil, Int. J. Multiph. Flow 51 (2013) 33–43.
[239] M.-R. Pendar, E. Roohi, Cavitation characteristics around a sphere: An LES investigation, Int. J. Multiph. Flow 98 (2018) 1–23.
[240] A. Kolahan, E. Roohi, M.-R. Pendar, Wavelet analysis and frequency spectrum of cloud cavitation around a sphere, Ocean Eng. 182 (2019) 235–247.
[241] H. Kato, T. Miyazawa, S. Timaya, T. Iwasaki, A STUDY OF AN AIR-LIFT PUMP FOR SOLID PARTICLES, Bulletin of JSME. 18 (1975) 286–294.
[242] E. Roohi, A.P. Zahiri, M. Passandideh-Fard, Numerical simulation of cavitation around a two-dimensional hydrofoil using VOF method and LES turbulence model, App. Math. Model. 37 (2013) 6469–6488.
[243] F.M. Owis, A.H. Nayfeh, Numerical simulation of 3-D incompressible, multi-phase flows over cavitating projectiles, Eur. J. Mech. B. Fluids 23 (2004) 339–351.
[244] J.-W. Suh, J.-W. Kim, Y.-S. Choi, J.-H. Kim, W.-G. Joo, K.-Y. Lee, Development of numerical Eulerian-Eulerian models for simulating multiphase pumps, J. Pet. Sci. Eng. 162 (2018) 588–601.
[245] D. Hirche, F. Birkholz, O. Hinrichsen, A hybrid Eulerian-Eulerian-Lagrangian model for gas-solid simulations, Chem. Eng. J. 377 (2019), 119743.
[246] Z. Wen, L. Zhang, H. Tang, J. Zeng, X. He, Z. Yang, Y. Zhao, A review on numerical simulation of proppant transport: Eulerian-Lagrangian views, J. Pet. Sci. Eng. 217 (2022), 110902.
[247] F. Garoosi, M.R. Safaei, M. Dahari, K. Hooman, Eulerian-Lagrangian analysis of solid particle distribution in an internally heated and cooled air-filled cavity, Appl. Math Comput. 250 (2015) 28–46.
[248] A. Andreini, C. Bianchini, S. Puggelli, F.X. Demoulin, Development of a turbulent liquid flux model for Eulerian-Eulerian multiphase flow simulations, Int. J. Multiph. Flow 81 (2016) 88–103.
[249] L. Hua, H. Zhao, J. Li, J. Wang, Q. Zhu, Eulerian-Eulerian simulation of irregular particles in dense gas–solid fluidized beds, Powder Technol. 284 (2015) 299–311.
[250] S. Elghobashi, On predicting particle-laden turbulent flows, Appl. Sci. Res. 52 (1994) 309–329.
[251] P.J. Zwart, A.G. Gerber, T. Belamri, A two-phase flow model for predicting cavitation dynamics, (2004).
[252] S. Frikha, O. Coutier-Delgosha, J.A. Astolfi, Influence of the Cavitation Model on the Simulation of Cloud Cavitation on 2D Foil Section, Int. J. Rotating Mach. 2008 (2008) 1–12.
[253] A.K. Singhal, M.M. Athavale, H. Li, Y. Jiang, Mathematical Basis and Validation of the Full Cavitation Model, J. Fluids Eng. 124 (2002) 617–624.
[254] G. Schnerr Professor Dr.-Ing.habil, Physical and Numerical Modeling of Unsteady Cavitation Dynamics, 2001.
[255] P.G. Saffman, On the stability of laminar flow of a dusty gas, J. Fluid Mech. 13 (1962) 120–128.
[256] G. Hetsroni, Particles-turbulence interaction, Int. J. Multiph. Flow 15 (1989) 735–746.
[257] S. Balachandar, J.K. Eaton, Turbulent Dispersed Multiphase Flow, Annu. Rev. Fluid Mech. 42 (2010) 111–133.
[258] C.T. Crowe, On models for turbulence modulation in fluid–particle flows, Int. J. Multiph. Flow 26 (2000) 719–727.
[259] D. Li, The Research on Numerical Simulation and Abrasion Property of Solid-liquid Two-phase-flow Centrifugal Pump, Zhejiang Sci-Tech University, 2014. Thesis.
[260] W. Dong, Numerical Simulation of Solid-liquid Two-phase Flow in Centrifugal Pump Based on the Particle, Zhejiang Sci-Tech University, 2015. Thesis.
[261] Y. Sato, K. Sekoguchi, Liquid velocity distribution in two-phase bubble flow, Int. J. Multiph. Flow 2 (1975) 79–95.
[262] J. Wang, Y. Wang, H. Liu, H. Huang, L. Jiang, An improved turbulence model for predicting unsteady cavitating flows in centrifugal pump, Int. J. Numer. Meth. Heat Fluid Flow 25 (2015) 1198–1213.
[263] H. Liu, J. Wang, Y. Wang, H. Zhang, H. Huang, Influence of the empirical coefficients of cavitation model on predicting cavitating flow in the centrifugal pump, Int. J. Naval Architecture Ocean Eng. 6 (2014) 119–131.
[264] L. Zhou, Z. Wang, Numerical Simulation of Cavitation Around a Hydrofoil and Evaluation of a RNG κ-ε Model, J. Fluids Eng. 130 (2008), 011302.
[265] D. Zhang, W. Shi, D. Pan, M. Dubuisson, Numerical and Experimental Investigation of Tip Leakage Vortex Cavitation Patterns and Mechanisms in an Axial Flow Pump, J. Fluids Eng. 137 (2015), 121103.
[266] C.K.W. Tam, The drag on a cloud of spherical particles in low Reynolds number flow, J. Fluid Mech. 38 (1969) 537–546.
[267] N. Zuber, On the dispersed two-phase flow in the laminar flow regime, Chem. Eng. Sci. 19 (1964) 897–917.
[268] S. Yuan, P. Zhang, J. Zhang, W. Xu, Numerical simulation of 3-d dense solid-liquid two-phase turbulent flow in a non-clogging mud pump, Chinese Journal of, Mech. Eng. 17 (2004) 623–627.
[269] K. Alawadhi, B. Alzuwayer, M. Alrahmani, A. Murad, Evaluation of the Erosion Characteristics for a Marine Pump Using 3D RANS Simulations, Appl. Sci. 11 (2021) 7364.
[270] I. Finnie, Erosion of surfaces by solid particles, Wear 3 (1960) 87–103.
[271] An experimental investigation of certain aerodynamic effects on erosion, Aerodynamic Testing Conference. (n.d.).
[272] Y.I. Oka, K. Okamura, T. Yoshida, Practical estimation of erosion damage caused by solid particle impact: Part 1: Effects of impact parameters on a predictive equation, Wear 259 (2005) 95–101.
[273] Y.I. Oka, T. Yoshida, Practical estimation of erosion damage caused by solid particle impact: Part 2: Mechanical properties of materials directly associated with erosion damage, Wear 259 (2005) 102–109.
[274] B.S. McLaury, J. Wang, S.A. Shirazi, J.R. Shadley, E.F. Rybicki, Solid Particle Erosion in Long Radius Elbows and Straight Pipes, in: OnePetro, 1997.
[275] Y. Zhang, E.P. Reuterfors, B.S. McLaury, S.A. Shirazi, E.F. Rybicki, Comparison of computed and measured particle velocities and erosion in water and air flows, Wear 263 (2007) 330–338.
[276] R. Fortes, J.L. Reboud, L. Briancon, A phenomenological and numerical model for scaling the flow aggressiveness in cavitation erosion, Cavitation Erosion Workshop, Val de Reuil, France, 2004.
[277] M.H. Arabnejad, U. Svennberg, R.E. Bensow, Numerical assessment of cavitation erosion risk using incompressible simulation of cavitating flows, Wear 464–465 (2021), 203529.
[278] A. Peters, O. el Moctar, Numerical assessment of cavitation-induced erosion using a multi-scale Euler-Lagrange method, J. Fluid Mech. 894 (2020) A19.
[279] A. Peters, O. el Moctar, Numerical assessment of cavitation-induced erosion using a multi-scale Euler-Lagrange method, J. Fluid Mech. 894 (2020).
[280] S. Chitrakar, B.W. Solemslie, H.P. Neopane, O.G. Dahlhaug, Review on numerical techniques applied in impulse hydro turbines, Renew. Energy 159 (2020) 843–859.
[281] M. Amir, A combined CFD-experimental method for developing an erosion equation for both gas-sand and liquid-sand flows, The University of Tulsa, 2016 thesis.
[282] C. Trivedi, O.G. Dahlhaug, A Comprehensive Review of Verification and Validation Techniques Applied to Hydraulic Turbines, Int. J. Fluid Mach. Syst. 12 (2019) 345–367.
[283] R. Koirala, B. Thapa, H.P. Neopane, B. Zhu, A review on flow and sediment erosion in guide vanes of Francis turbines, Renew. Sustain. Energy Rev. 75 (2017) 1054–1065.
[284] Y.-M. Chen, J. Mongis, Cavitation wear in plain bearing: Case study, Mech. Ind. 6 (2005) 195–201.
[285] Y. Tianchen, A Review of the Research on the Influence of Cavitation and Abrasion on Hydroturbine Performance, E3S Web Conf. 233 (2021) 03068.
[286] H. Yu, Y.G. Zheng, Z.M. Yao, The cavitation erosion and erosion-corrosion behavior of carbon steel in simulating solutions of three rivers of China, Mater. Corros. 57 (2006) 705–714.
[287] J.F. Santa, L.A. Espitia, J.A. Blanco, S.A. Romo, A. Toro, Slurry and cavitation erosion resistance of thermal spray coatings, Wear 267 (2009) 160–167.
[288] R. Singh, D. Kumar, S.K. Mishra, S.K. Tiwari, Laser cladding of Stellite 6 on stainless steel to enhance solid particle erosion and cavitation resistance, Surf. Coat. Technol. 251 (2014) 87–97.

[289] K. Kumar, R.P. Saini, Development of correlation to predict the efficiency of a hydro machine under different operating conditions, Sustainable Energy Technol. Assess. 50 (2022), 101859.
[290] S. Poddar, N. Tandon, Classification and detection of cavitation, particle contamination and oil starvation in journal bearing through machine learning approach using acoustic emission signals, Proc. Inst. Mech. Eng., Part J: J. Eng. Tribol. 235 (2021) 2137–2143.
[291] A review on operation and maintenance of hydropower plants, Sustainable Energy Technologies and Assessments. 49 (2022) 101704.
[292] Y. Zhang, Q. Min, Y. Zhang, X. Du, Effects of liquid compressibility on bubble-bubble interactions between oscillating bubbles, J. Hydrodyn. 28 (2016) 832–839.
[293] Y. Zhang, S. Li, Improved formulas for thermal behavior of oscillating nanobubbles, J. Hydrodyn. Ser. B. 28 (2016) 325–328.
[294] R. Etchepare, H. Oliveira, M. Nicknig, A. Azevedo, J. Rubio, Nanobubbles: Generation using a multiphase pump, properties and features in flotation, Miner. Eng. 112 (2017).
[295] Y. Zhang, Z. Guo, X. Du, Wave propagation in liquids with oscillating vapor-gas bubbles, Appl. Therm. Eng. 133 (2018) 483–492.
[296] Y. Zhang, Y. Zhang, S. Li, Combination and simultaneous resonances of gas bubbles oscillating in liquids under dual-frequency acoustic excitation, Ultrason. Sonochem. 35 (2017) 431–439.